CHEMICAL KINETICS FOR TNF TARGET FLAMES
Benchmark of the main NH_3 and NH_3-H_2 kinetic mechanisms against a wide range of experimental data

Alessandro Stagni*, Timoteo Dinelli

Department of Chemistry, Materials, and Chemical Engineering "G. Natta", Politecnico di Milano, Milano 20133, Italy
**Corresponding author. email: alessandro.stagni@polimi.it*

Contents

1 Summary of experimental data

Mixture	Section	Experimental device	T [K]	P [atm]	Φ [-]	Ref.
		Laminar flame speed				
$NH_3/O_2/Ar$	4.1.1	Shock tube	477-771	1	0.75-1.25	[1]
$NH_3/H_2/O_2/Ar$	4.1.2	Shock tube	500-820	1	0.8-1.2	[2]
$NH_3/H_2/air$	4.1.3	Constant-volume chamber	298-473	1	0.8-1.4	[3]
$NH_3/H_2/O_2/N_2$	4.1.4	Constant-volume chamber	298-473	1-10	0.8-1.4	[4]
NH_3/air	4.1.5	Constant-volume chamber	400-500	1-5	0.8-1.2	[5]
$NH_3/H_2/N_2/air$	4.1.6	Constant-volume chamber	298	1-10	0.7-1.4	[6]
NH_3/O_2	4.1.7	Constant-volume chamber	298-473	0.5-1.6	0.5-2	[7]
$NH_3/O_2/N_2$	4.1.8	Constant-volume chamber	298	1-5	0.6-1.5	[8]
$NH_3/H_2/air$	4.1.9	Constant-volume chamber	298	1-5	0.8-1.8	[9]
$NH_3/O_2/N_2/He$	4.1.10	Constant-volume chamber	309-423	1	0.8-1.3	[10]
$NH_3/NO/N_2O/N_2$	4.1.11	Constant-volume chamber	298-473	1-7	0.7-1.9	[11]
$NH_3/H_2/air$	4.1.12	Constant-volume chamber	423	1-25	0.6-1.4	[12]
$NH_3/H_2/air$	4.1.13	Heat flux burner	298	1-5	0.7-1.4	[13]
		Extinction strain rates				
$NH_3/H_2/air$	4.2.1	Counterflow diffusion flame	See text	1	-	[14]
		Species measurements				
$NH_3/H_2/air$	4.3.1	Counterflow diffusion flame	See text	1	-	[14]
$NH_3/H_2/N_2/air$	4.3.2	Counterflow diffusion flame	290	1	-	[15]
$NH_3/H_2/air$	4.3.3	Burner-stabilized flame	295	1	0.57-1.4	[16]
$NH_3/H_2/N_2/air$	4.3.4	Flat flame burner	298	1	0.6-1.4	[17]
$NH_3/H_2/Ar$	4.3.5	Shock tube	2100-3000	1.2	∞	[18]
$NH_3/H_2/O_2/Ar$	4.3.6	Shock tube	1474-2307	1.2	0.56-2.07	[19]
$NH_3/O_2/Ar$	4.3.7	Shock tube	1829-2198	1.2	0.5-1.8	[20]
$NH_3/N_2O/Ar$	4.3.8	Shock tube	1458-2200	1.25-1.47	0.25-2	[21]

Table 1: Experimental data used for model validation. For laminar flame speed and burner-stabilized flame, T indicates the mixture inlet temperature T_u.

2 Numerical tools

The numerical simulations were performed using the `Cantera` v3.2.0 [22] and `OpenSMOKE++` suite of solvers [23], developed at CRECK Modeling, Politecnico di Milano. Both codes were previously successfully cross-validated [24]. The ideal-reactor configurations were modeled through the following approaches:

i. **Shock Tubes**: adiabatic, constant-volume batch reactors were considered. When a pressure profile was available from the related experiments, this was imposed to the simulations.

ii. **Premixed laminar flames**: an adaptive mesh refinement method was adopted solving a 5-cm grid, and setting maximum allowed gradient and curvature coefficients between adjacent points at 0.02 and 0.1, respectively. Radiative heat losses, shown to be significant for ammonia flames [25, 26], were accounted for using an optically-thin model, considering contributions from H_2O as well as NH_3, NO and N_2O. Cantera v3.2.0 was properly extended to include radiation contributions from nitrogen-containing species. Multicomponent transport and Soret effects were accounted for. For visualization purposes, laminar flame speed trends were represented using spline-smoothed curves based on the discrete simulation points; when too few points were available, the original data were plotted without smoothing.

iii. **Burner-stabilized stagnation flames**: an adaptive mesh refinement method was adopted, setting maximum allowed gradient and curvature coefficients between adjacent points at 0.05 and 0.1, respectively, with a pruning coefficient of 0.02. Radiative heat losses were accounted for using an optically-thin model, considering contributions from H_2O as well as NH_3, NO and N_2O, activated after multicomponent transport to avoid solver resets. Multicomponent transport and Soret effects were accounted for. A staged solution strategy was adopted to ensure convergence: the energy equation was initially disabled on a fixed grid with mixture-averaged transport, then progressively enabled with grid refinement, before switching to multicomponent transport with Soret effect accounted for, and finally activating radiation. Solution continuation across equivalence ratios was employed whenever available, using the converged solution from the previous case as initial guess.

iv. **Counterflow flames**: a two-stage mesh refinement strategy was adopted, with a coarse pass (*slope = 0.15, curve = 0.25*) followed by a fine pass (*slope = 0.06, curve = 0.12*). A staged solution strategy was employed: the energy equation was initially disabled with mixture-averaged transport, then enabled with the coarse refinement criteria, before switching to multicomponent transport with Soret effect included and finally activating radiation, the latter two solved with the fine criteria. The extinction strain rate was determined via a continuation procedure: starting from a converged solution at a strain rate well above the lower extinction limit, the strain rate was ramped upward in relative increments of 1%. Upon solver failure or detection of a cold solution (Tmax $<$ 500 K), the increment was halved and the last converged solution was restored; this bisection was repeated until the relative increment fell below 0.01%, at which point the last successful strain rate was taken as the extinction value.

3 Kinetic mechanisms

The following mechanisms were considered for validation:

1. `C3MechLite V4.0.1`: available in the work of Murakami et al. [27], it was based on the previous work of Zhu et al. [28], and is a reduced version of the larger C3MechV4.0.1 [29]. It is made up of 25 species and 164 reactions. The `yaml` file was used for Cantera simulations, while for OpenSMOKE++, the CHEMKIN files were directly used. Link: `https://github.com/C3Mech/C3Mech_reduced/tree/main/C3MechLite`.

2. `CRECK 2025`: available in the work of Stagni and Dinelli [30], it was based on the previous works by the same research group [31, 32]. It is made of 34 species and 273 reactions. The `yaml` file available as Supplemental Material was used for Cantera simulations, while for OpenSMOKE++, the CHEMKIN files were directly used. Link: `https://doi.org/10.1016/j.cej.2025.170737`.

3. `KAUST 2024`: available in the work of Monge-Palacios et al. [33], updated from the previous work of Zhang et al. [34]. It is made up of 36 species and 274 reactions. To run in Cantera, it was converted directly from the CHEMKIN files. Link: `https://doi.org/10.1016/j.pecs.2024.101177`.

4 Mechanisms validation

4.1 Laminar flame speed

4.1.1 Figueroa-Labastida (2024) [1]

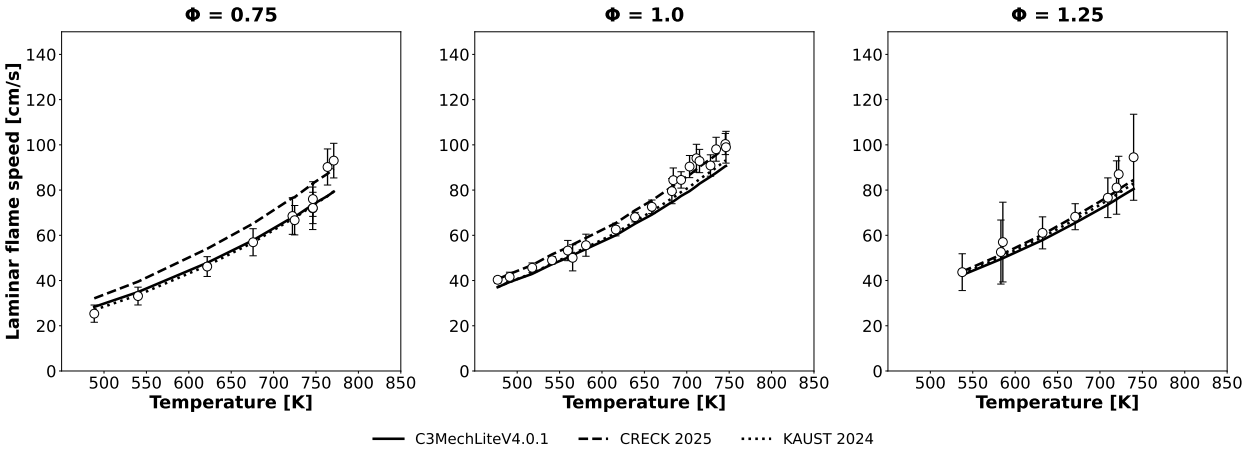

Figure 1: Laminar flame speed of $NH_3/O_2/Ar$ ($X_{O_2}/X_{Ar} = 79/21$) mixtures at atmospheric pressure and variable T_u and Φ.

4.1.2 Figueroa-Labastida (2024) [2]

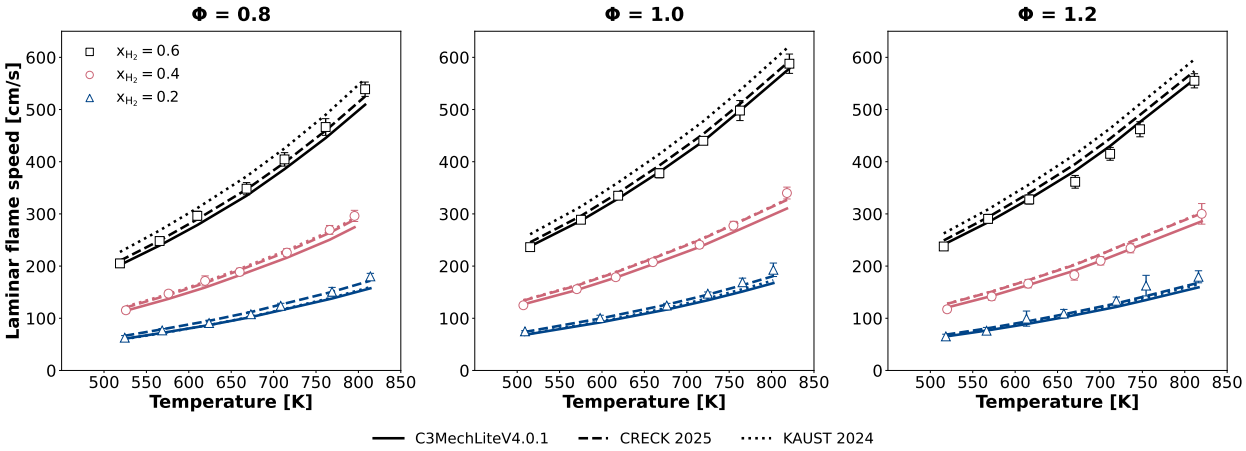

Figure 2: Laminar flame speed of $NH_3/H_2/O_2/Ar$ ($X_{O_2}/X_{Ar} = 79/21$) mixtures at atmospheric pressure and variable T_u and Φ.

4.1.3 Lhuillier (2020) [3]

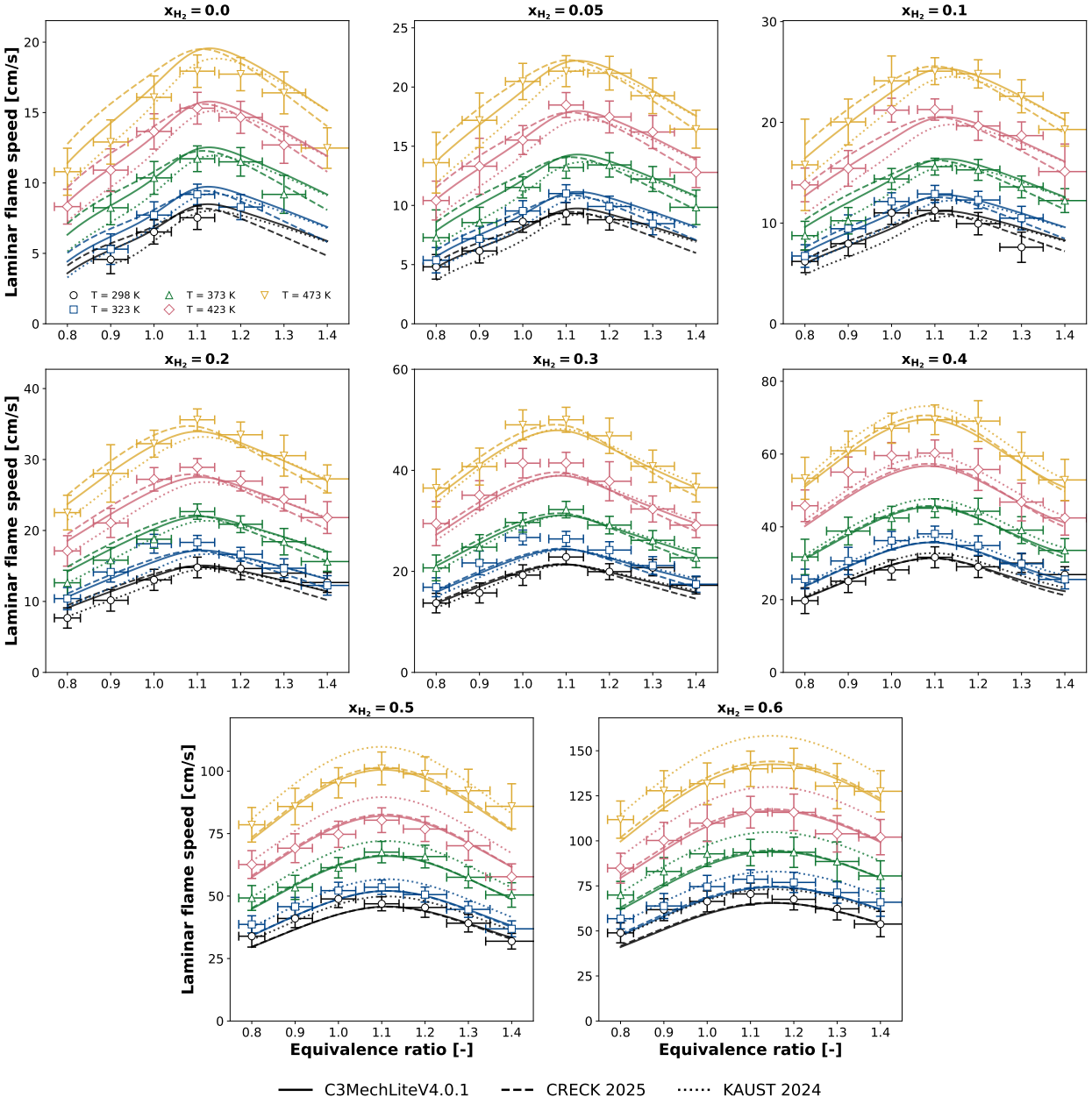

Figure 3: Laminar flame speed of NH_3/air mixtures at atmospheric pressure and variable X_{H_2} in the fuel, T_u. Variation with Φ.

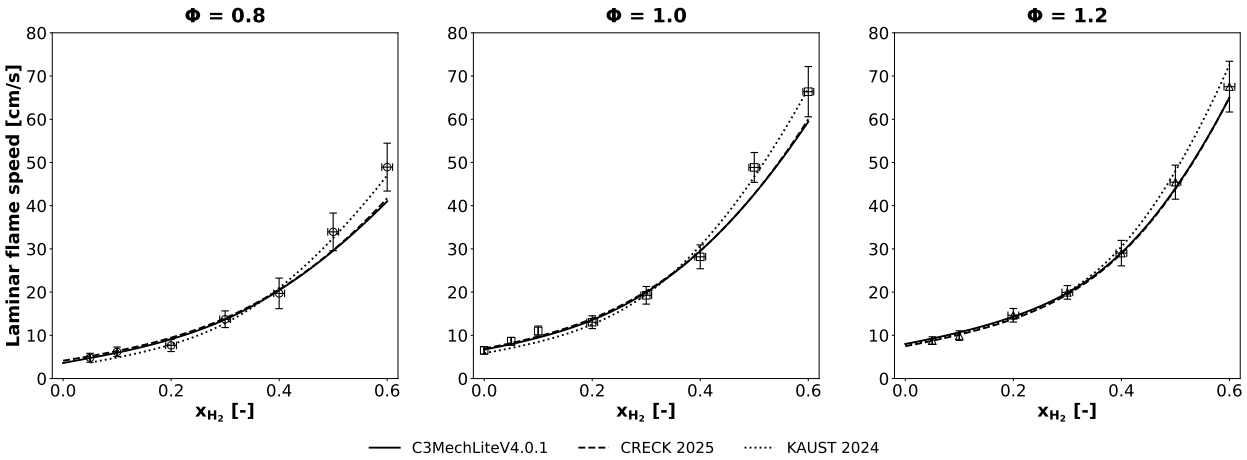

Figure 4: Laminar flame speed of NH_3/air mixtures at atmospheric pressure and temperature, for fixed Φ values. Variation with X_{H_2}.

4.1.4 Shrestha (2021) [4]

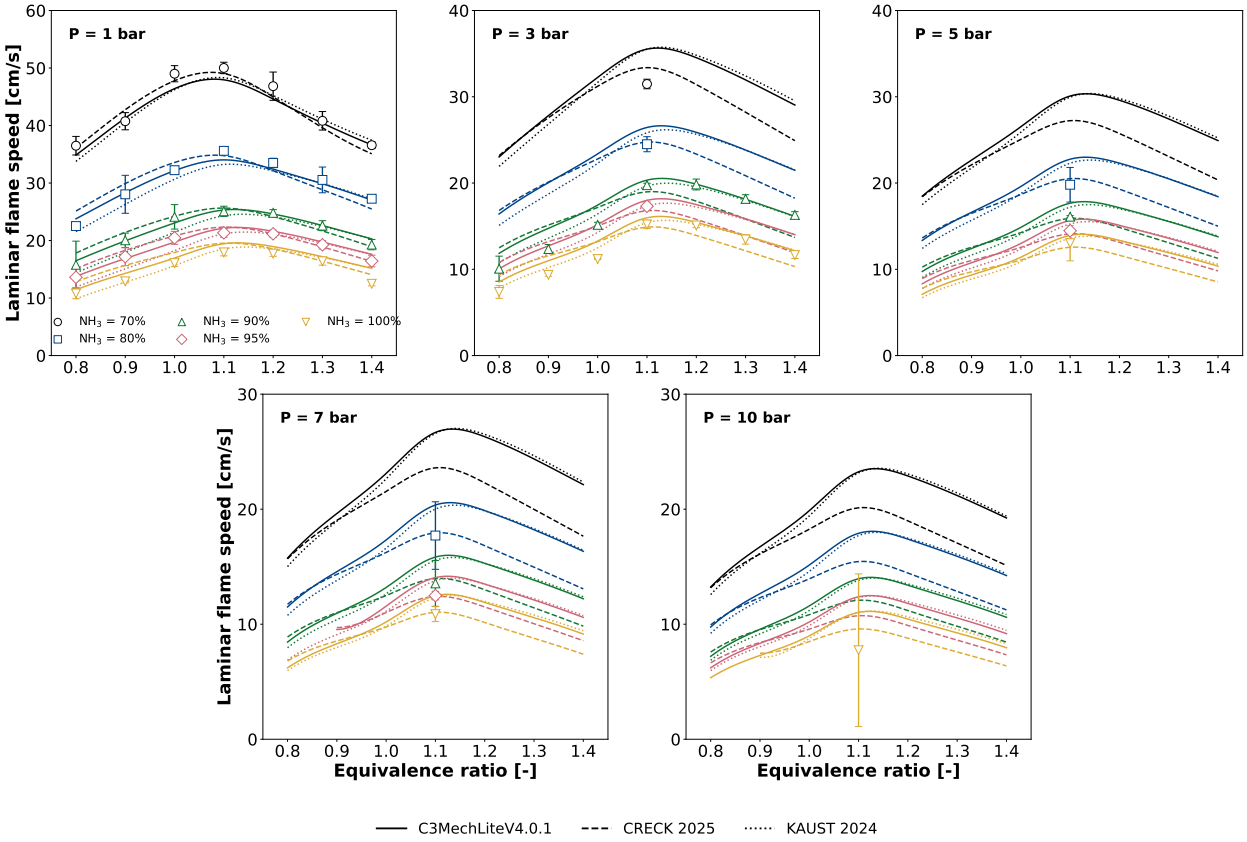

Figure 5: Laminar flame speed of $NH_3/H_2/air$ mixtures at variable P and Φ. $T_u = 473$ K.

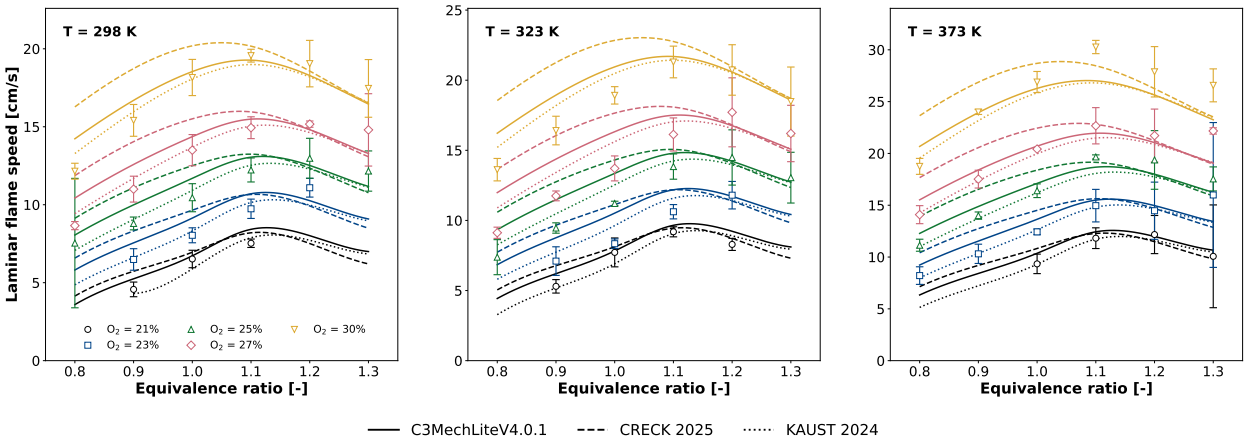

Figure 6: Laminar flame speed of $NH_3/O_2/N_2$ mixtures at atmospheric pressure and variable X_{O_2} in the oxidizer (balance N_2), T_u and Φ.

4.1.5 Kanoshima (2022) [5]

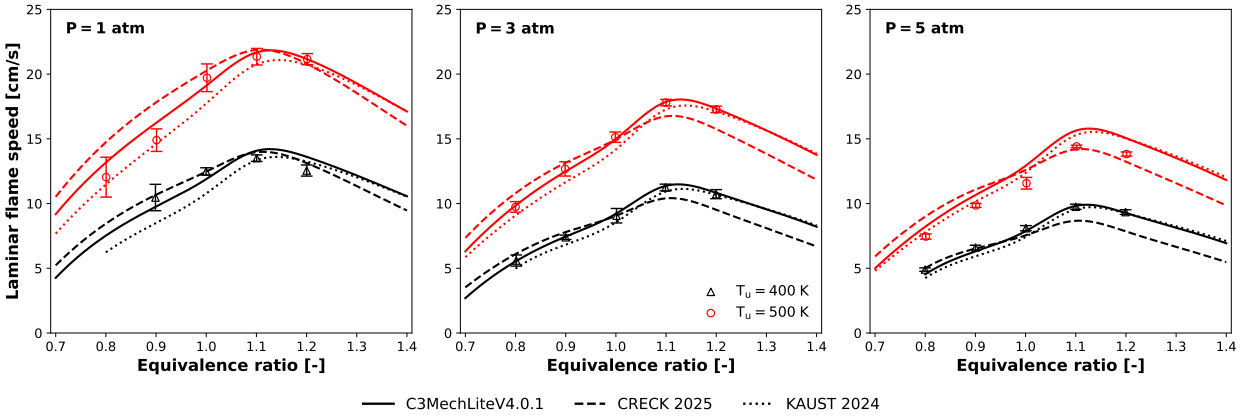

Figure 7: Laminar flame speed of NH_3/air mixtures at variable P and T_u.

4.1.6 Mei (2021) [6]

In the following, partially cracked NH_3 is investigated at variable P, Φ and cracking fraction γ. This is defined in Eq. 1 as in the reference work [5]:

$$\gamma = \frac{[NH_3]_{cracked}}{[NH_3]_0} = \frac{2[H_2]}{3[NH_3] + 2[H_2]} \tag{1}$$

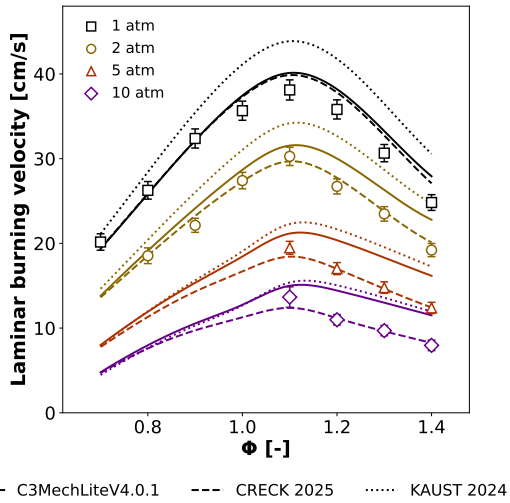

Figure 8: Laminar flame speed of cracked NH_3/air mixtures at variable P and Φ. $T_u = 298$ K. $\gamma = 40$ %.

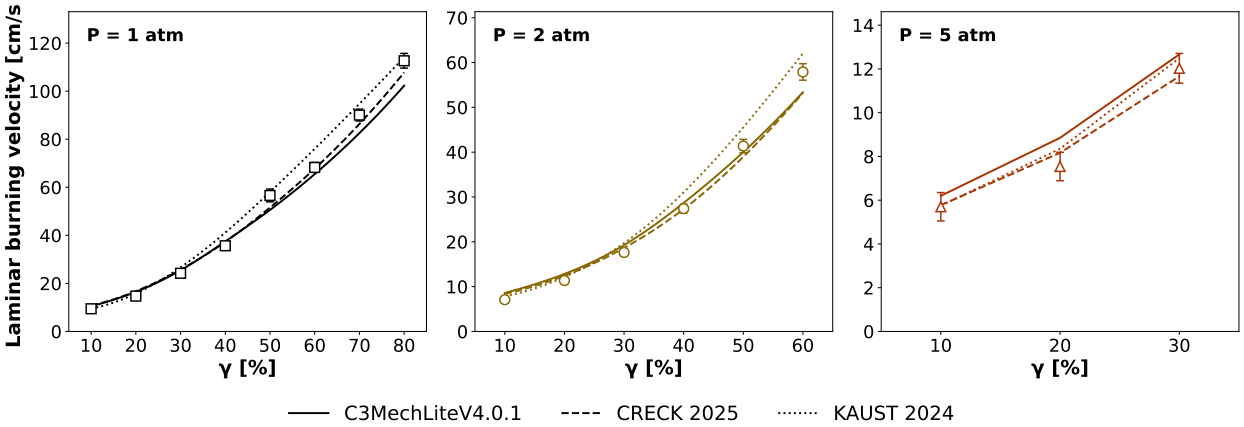

Figure 9: Laminar flame speed of cracked NH_3/air mixtures at variable P and γ. $T_u = 298$ K. $\Phi = 1$.

4.1.7 Liu (2019) [7]

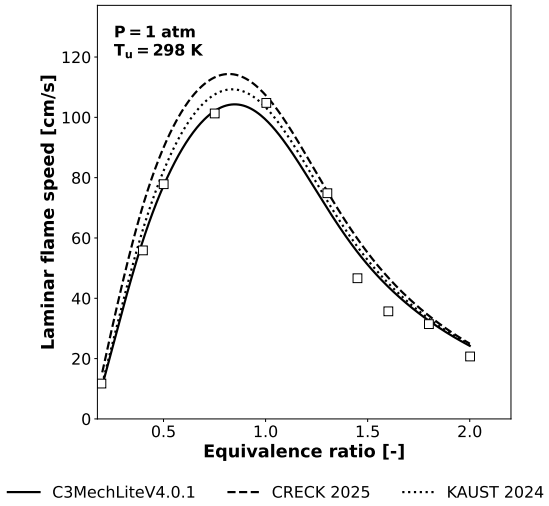

Figure 10: Laminar flame speed of NH_3/O_2 mixtures at atmospheric pressure and temperature, and variable Φ.

4.1.8 Mei (2019) [8]

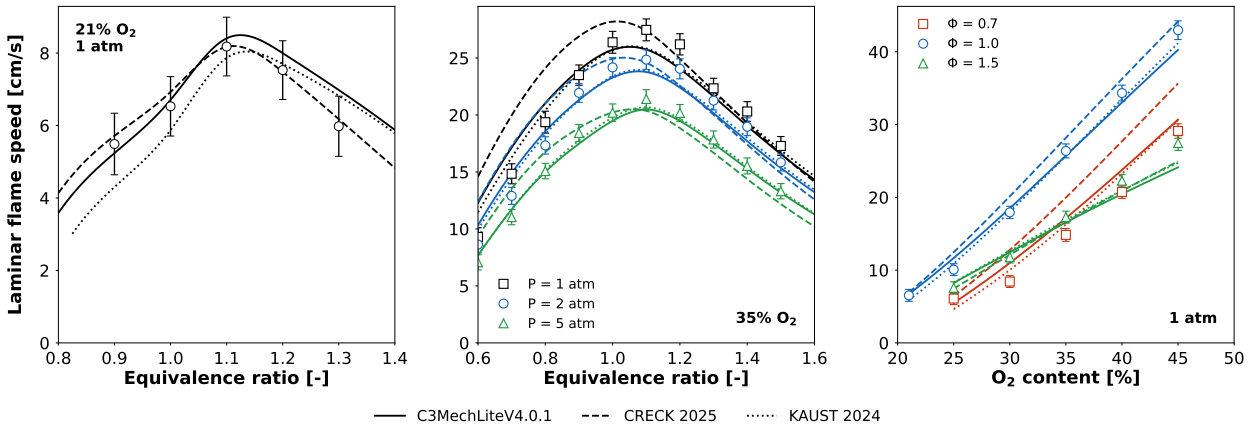

Figure 11: Laminar flame speed of $NH_3/O_2/N_2$ mixtures at variable pressure and variable X_{O_2} in the oxidizer (balance N_2), and Φ. $T_u = 298$ K.

4.1.9 Gotama (2022) [9]

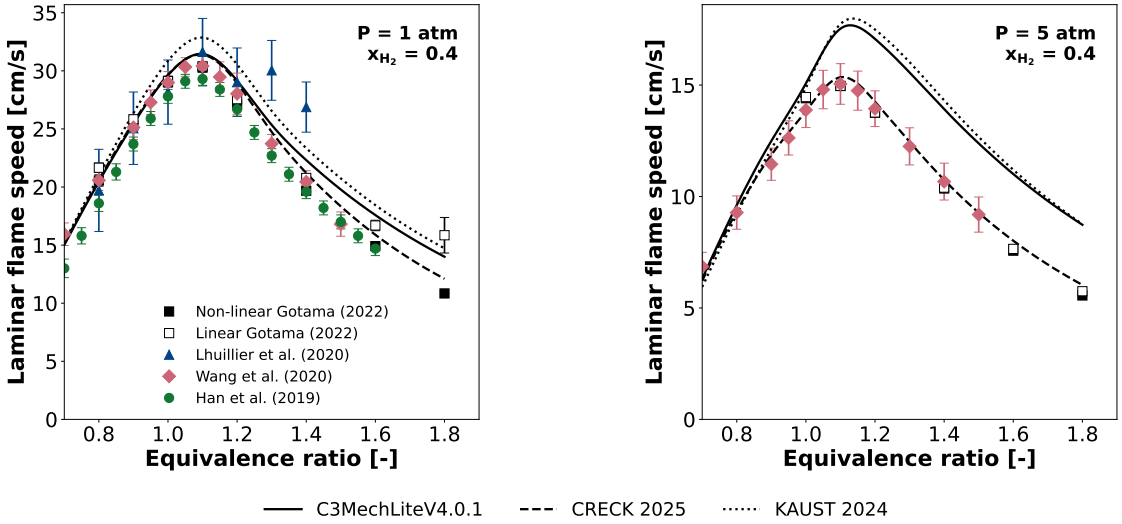

Figure 12: Laminar flame speed of NH_3/H_2/air mixtures at T_u = 298 K and variable P. X_{H_2} = 0.4. For completeness, experiments by other authors [3, 13, 35] performed at the same conditions are shown.

4.1.10 Hamadi (2024) [10]

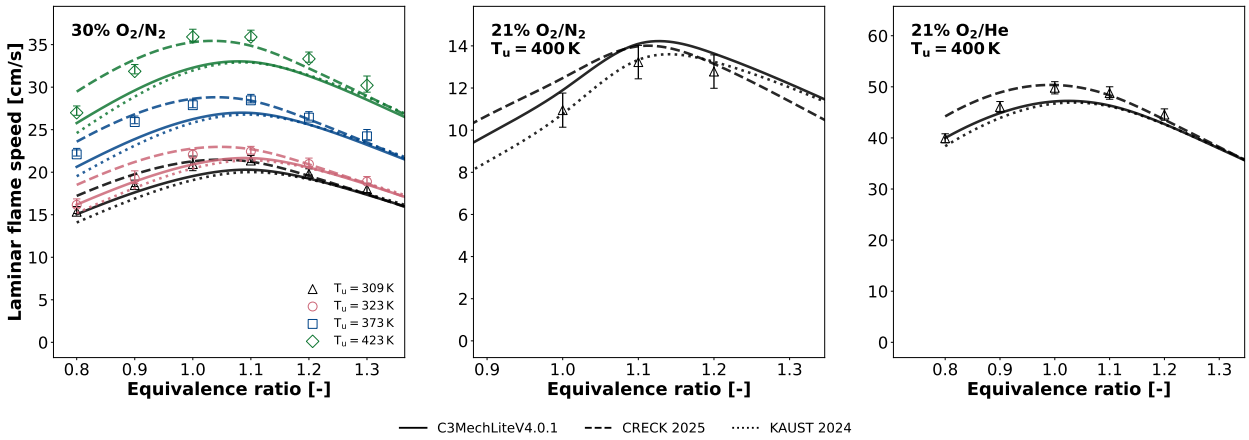

Figure 13: Laminar flame speed of $NH_3/O_2/N_2$ and $NH_3/O_2/He$ mixtures at atmospheric pressure and variable T_u.

4.1.11 Liu (2025) [11]

In the following, the equivalence ratio was calculated through the following global reactions:

$4NH_3 + 6(NO + N_2) = 6H_2O + 11N_2$

$2NH_3 + 3(N_2O + N_2) = 3H_2O + 7N_2$

such that

$\Phi = \frac{X_{NH_3}}{X_{NO/N_2O}} / \left[\frac{X_{NH_3}}{X_{NO/N_2O}}\right]_{stoich}$

The content of NO and N_2O, respectively, (Ra_{N_iO}) is defined as follows:

$Ra_{N_iO} = \frac{X_{N_iO}}{X_{N_iO}+X_{N_2}}$

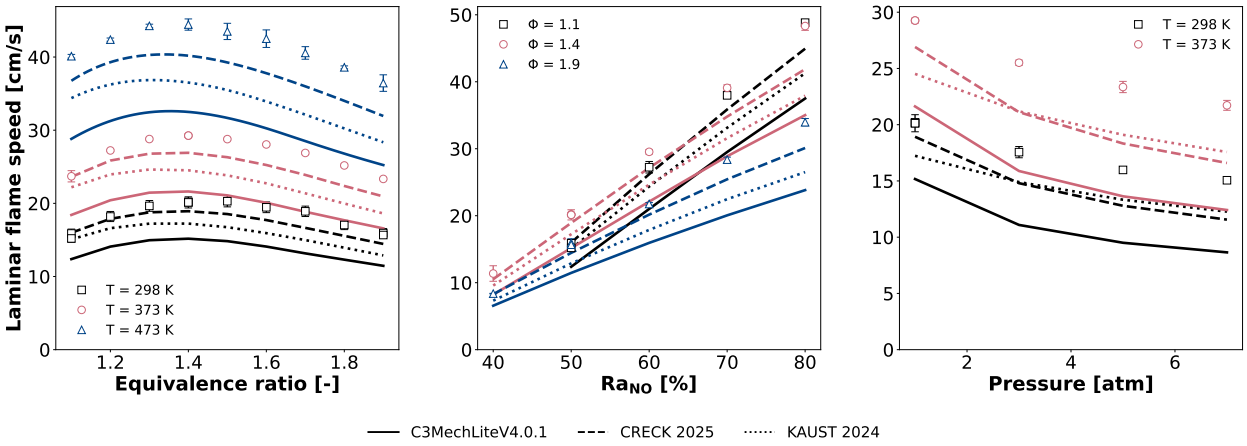

Figure 14: Laminar flame speeds of $NH_3/NO/N_2$ blends at variable Φ, T_u, Ra_{NO} and P.

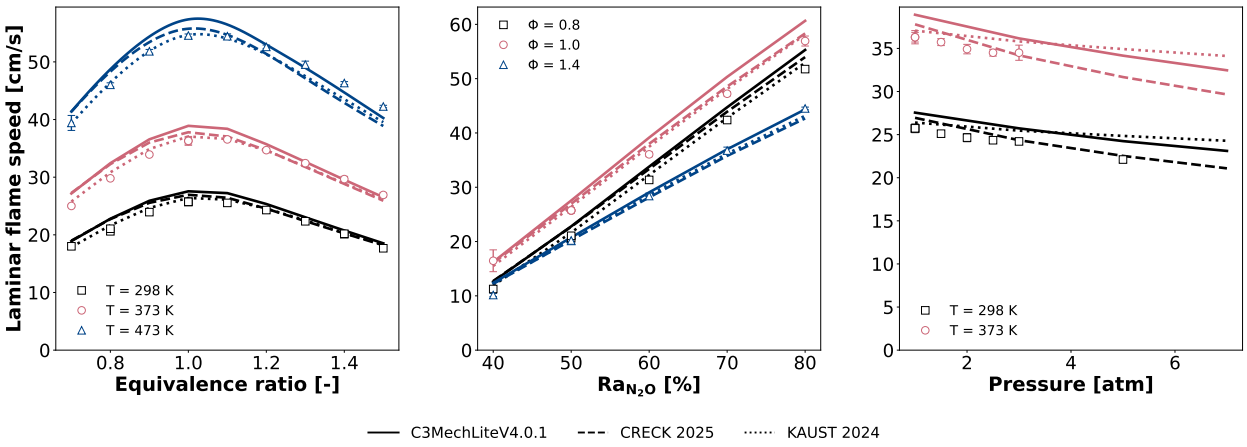

Figure 15: Laminar flame speeds of $NH_3/N_2O/N_2$ blends at variable Φ, T_u, Ra_{N_2O} and P.

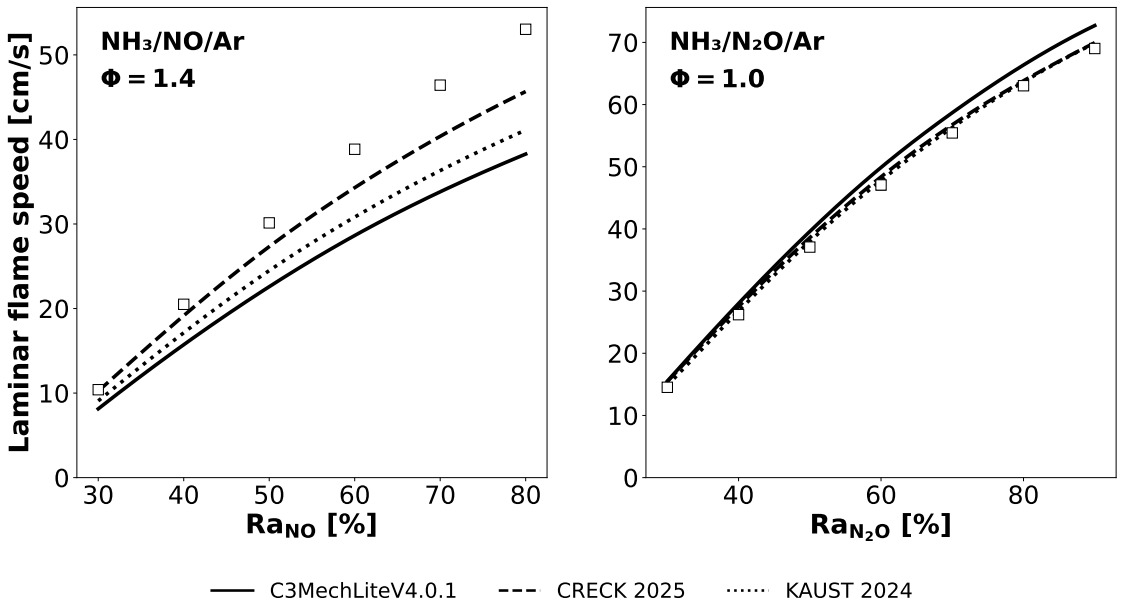

Figure 16: Laminar flame speeds of NH_3/NO/Ar and NH_3/N_2O/Ar blends at atmospheric pressure and temperature, and variable Ra_{N_iO}.

4.1.12 Wang (2024) [12]

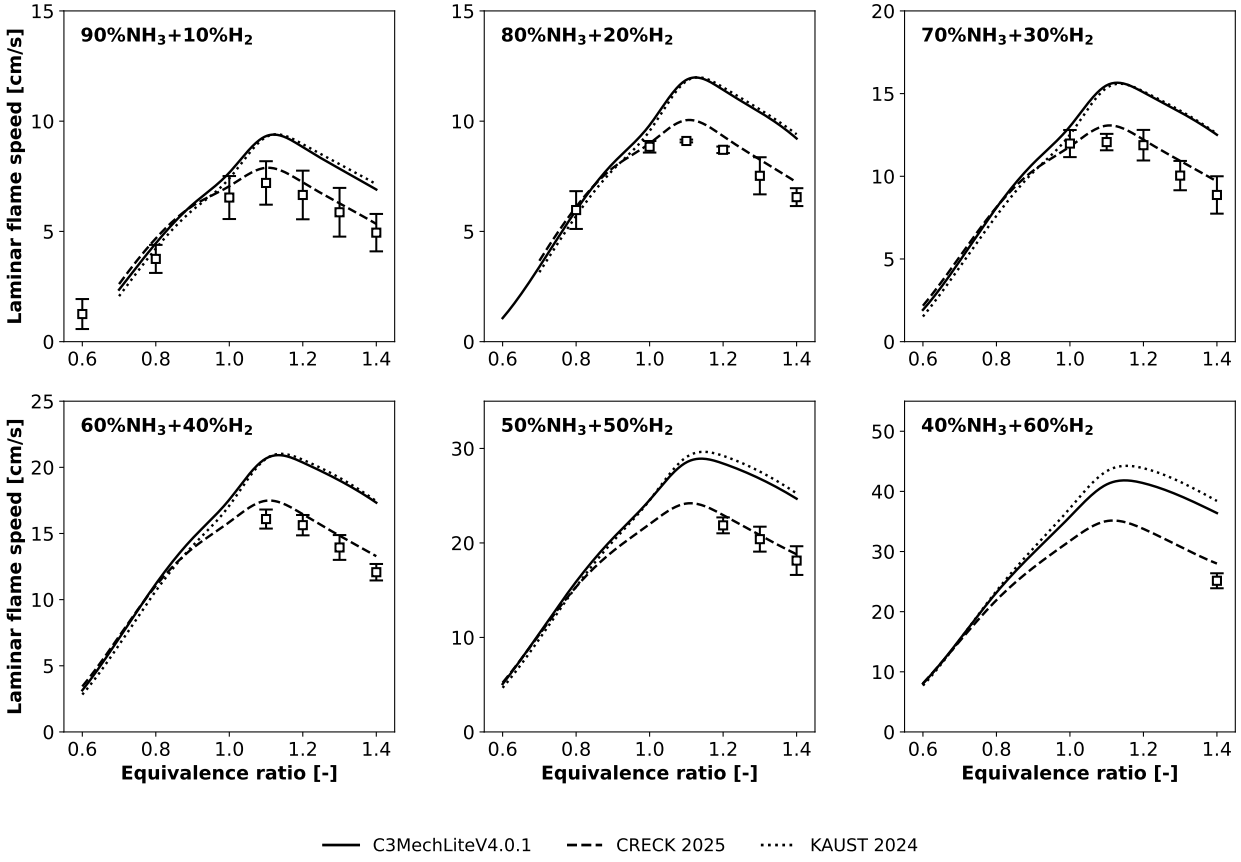

Figure 17: Laminar flame speed of NH_3/H_2/air mixtures at T_u = 423 K, P = 1.5 MPa and variable Φ and X_{H_2}.

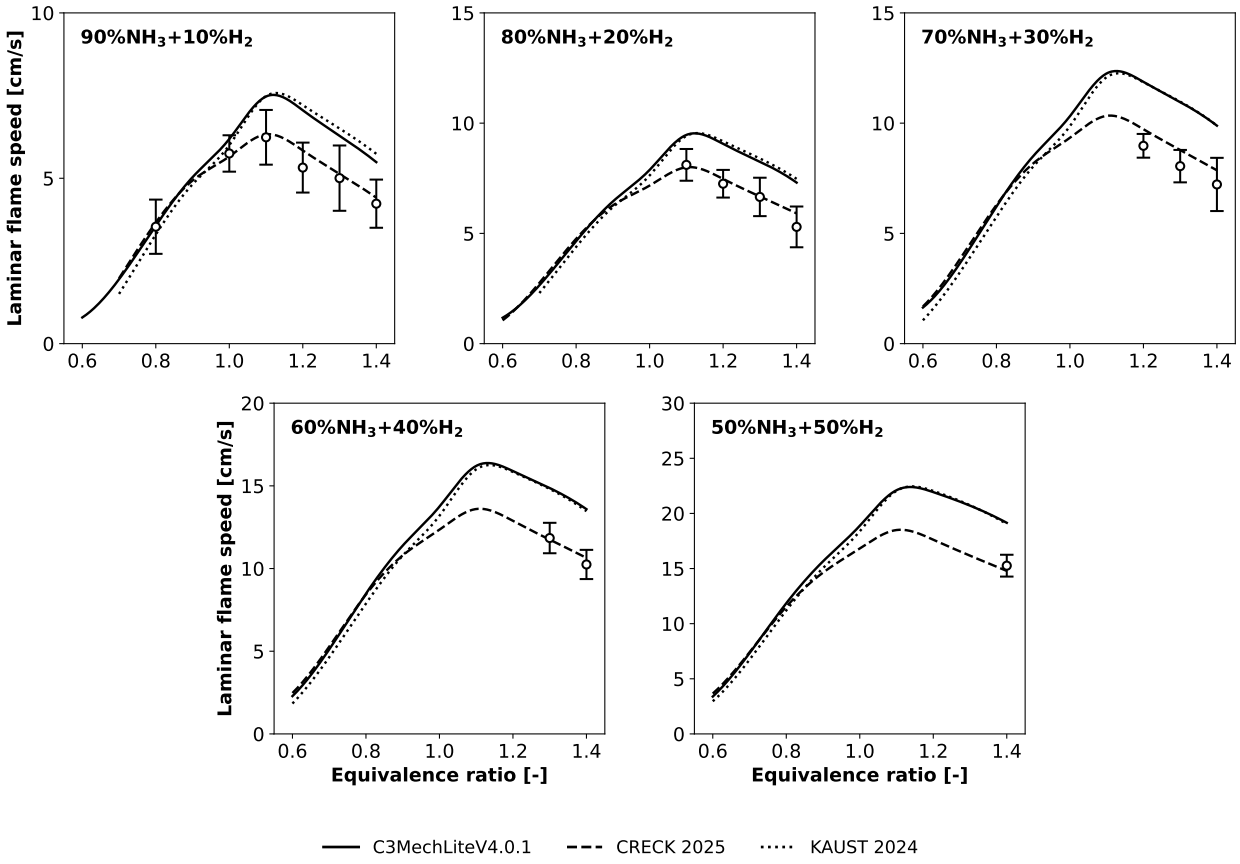

Figure 18: Laminar flame speed of NH_3/H_2/air mixtures at T_u = 423 K, P = 2.5 MPa and variable Φ, for fixed X_{H_2}.

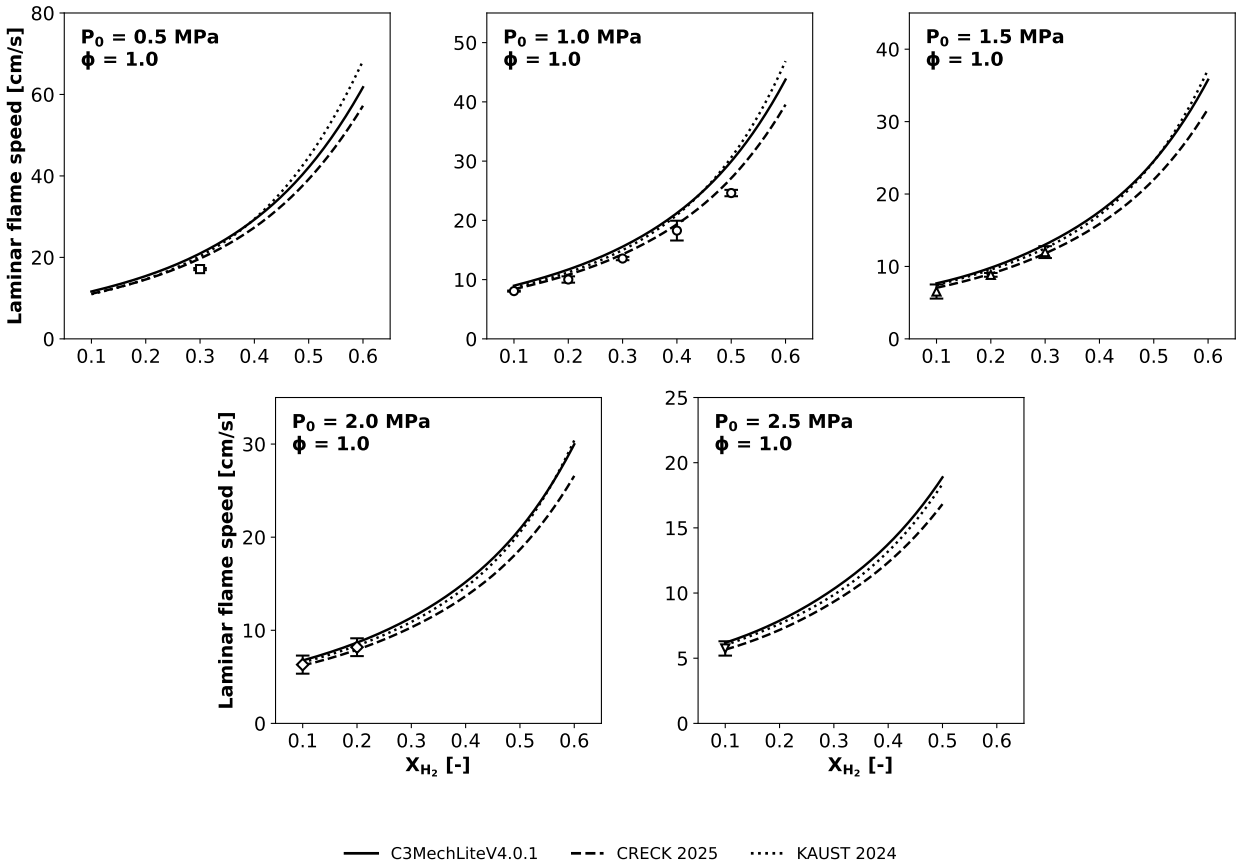

Figure 19: Laminar flame speed of NH_3/H_2/air mixtures at T_u = 423 K, and variable X_{H_2}, for fixed Φ and pressure.

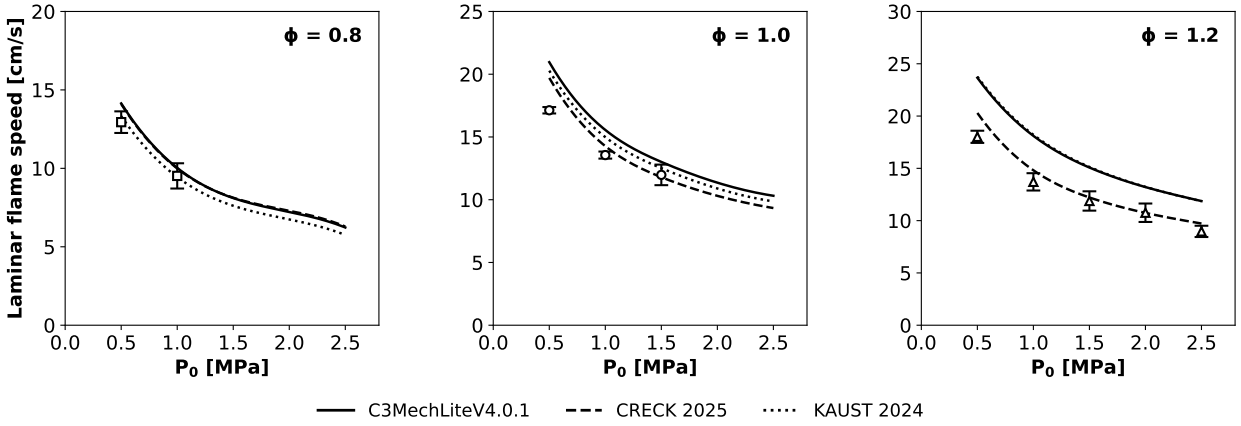

Figure 20: Laminar flame speed of NH_3/H_2/air mixtures at T_u = 423 K, and variable pressure, for fixed Φ. X_{H_2} = 0.3.

4.1.13 Wang (2020) [13]

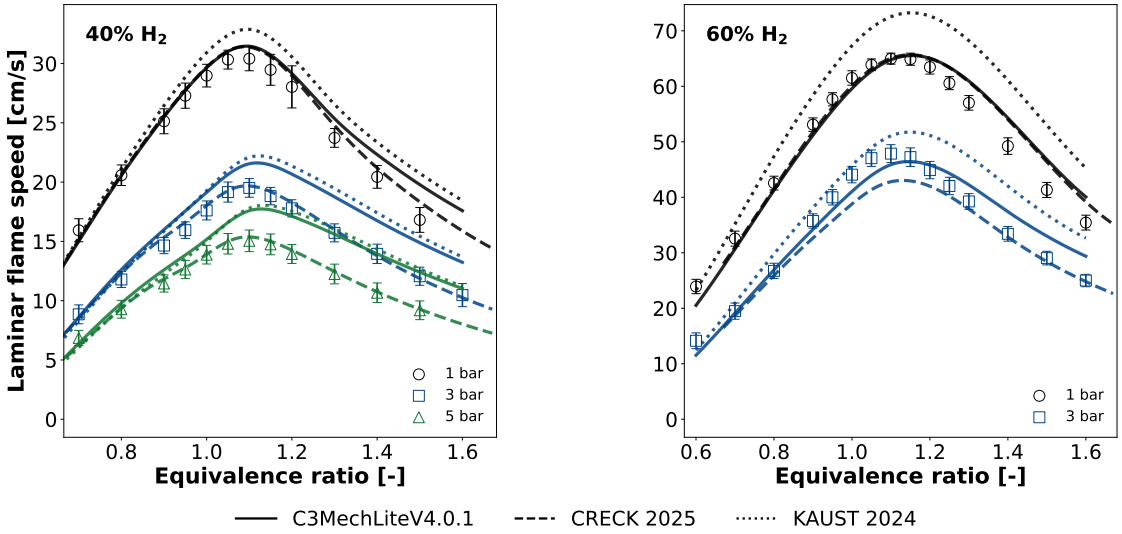

Figure 21: Laminar flame speed of NH_3/H_2/air mixtures at T_u = 298 K and variable P. X_{H_2} = 0.4 and 0.6.

4.2 Extinction strain rates

4.2.1 Thomas (2023) [14]

In the following, the effective strain rate a_{eff} is given in Eq. 2, as proposed in [11] based on the analysis of Seshadri and Williams [36]:

$$a_{eff} = \frac{2\,|u_w|}{L}\left(1 + \frac{u_f}{|u_w|}\sqrt{\frac{\rho_f}{\rho_o}}\right) \tag{2}$$

where L is the outlet separation distance, u_f is the fuel velocity, u_o the oxidizer velocity, and ρ_f and ρ_o the fuel and oxidizer densities, respectively. The fuel inlet temperature T_f is estimated as $T_f = 301 + 230\,e^{-0.057\,a_{eff}}$, while the oxidizer inlet temperature T_o is estimated as $T_o = 333 + 1040\,e^{-0.075\,a_{eff}}$. The oxidizer outlet velocity was calculated starting from the fuel outlet velocity to give approximately equal momentum for both flows, such to place the stagnation plane at half of the separation distance.

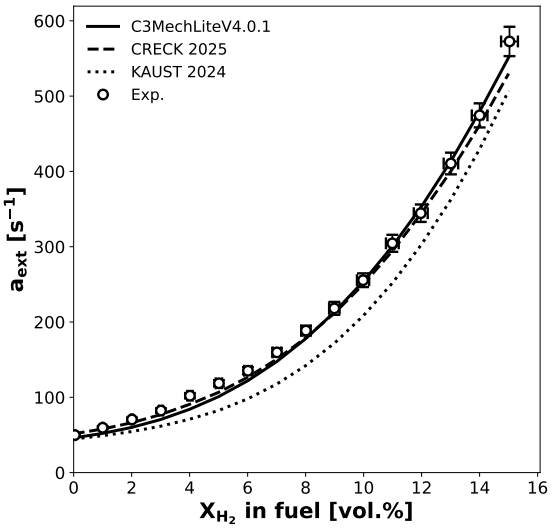

Figure 22: Extinction strain rates for NH_3/H_2 fuel blends in a counterflow flame. L = 10 mm. $X_{H_2} = 0 - 15\%$.

4.3 Species measurements

4.3.1 Thomas (2023) [14]

The geometries, operating parameters and modeling assumptions of this experimental campaign are defined in section 4.2.1.

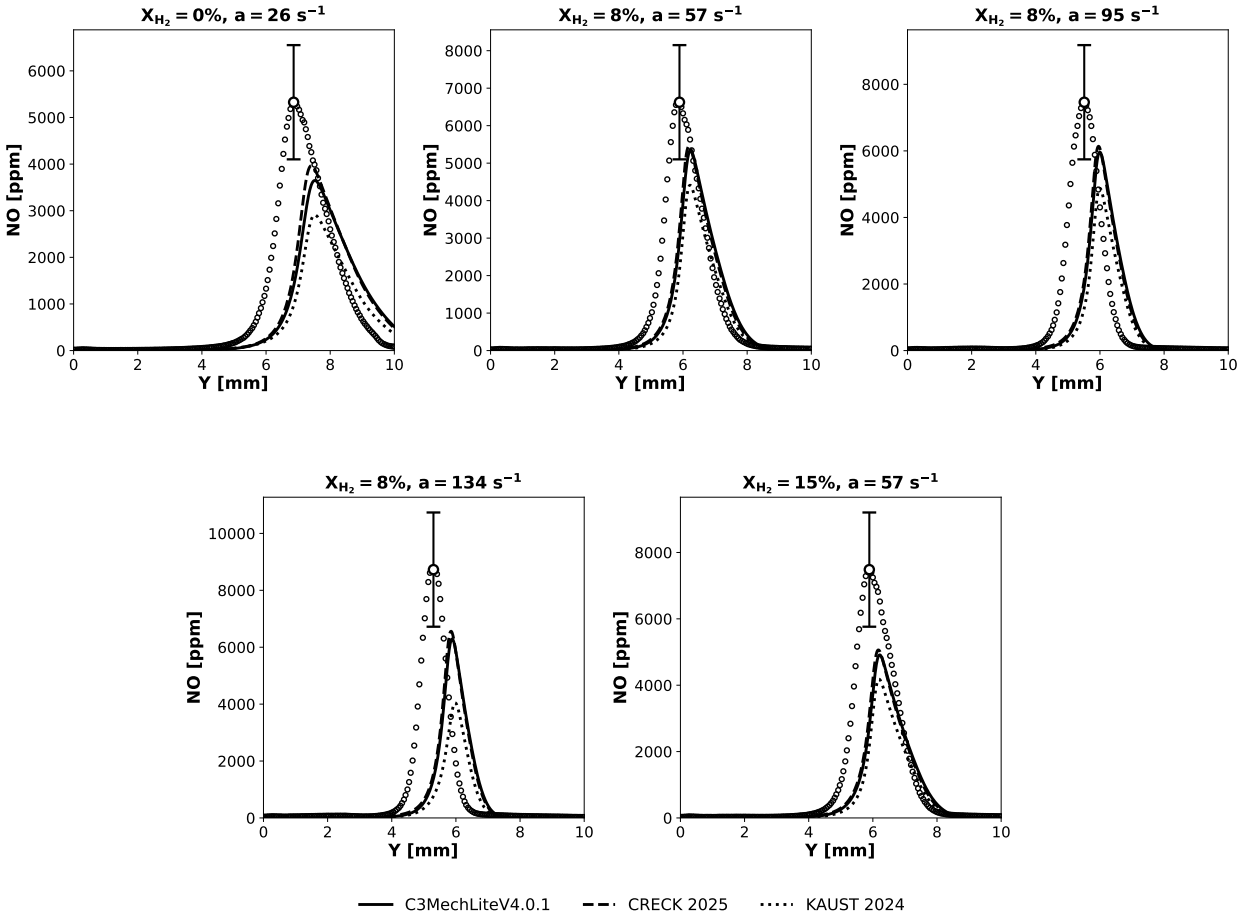

Figure 23: NO profiles in a counterflow diffusion flame at atmospheric pressure, and variable X_{H_2} and $a_e$ff.

4.3.2 Tang (2024) [15]

In the following, non-premixed flame simulations were performed as indicated in [15], i.e. by correcting U_{fuel} and U_{air} to match the corrected strain rate K_{fitted}. Detailed composition and parameters are listed in Table 2. For plotting, each experimental and modeling profile is aligned by shifting the x-axis so that $x = 0$ occurs at the location where the temperature first reaches half of its maximum. Distance between the two jets is 10 mm.

Case	$\mathbf{X_{NH_3}}$ [-]	$\mathbf{X_{H_2}}$ [-]	$\mathbf{X_{N_2}}$ [-]	$\mathbf{U_{fuel}}$ **(m/s)**	$\mathbf{U_{air}}$ **(m/s)**	**K (1/s)**	$\mathbf{K_{fitted}}$ (1/s)
AH82	0.80	0.20	-	0.60	0.40	100	80
AH64	0.60	0.40	-	0.60	0.40	100	80
AH46	0.40	0.60	-	0.62	0.38	100	75
N_0	0.50	0.50	0.00	0.60	0.40	100	75
N_08	0.46	0.46	0.08	0.60	0.40	100	75
N_16	0.42	0.42	0.16	0.60	0.40	100	75
N_24	0.38	0.38	0.24	0.60	0.40	100	75
N_30	0.35	0.35	0.30	0.60	0.40	100	75
AH64_K80	0.60	0.40	-	0.48	0.32	80	65
AH64_K120	0.60	0.40	-	0.72	0.48	120	85
AH64_K140	0.60	0.40	-	0.84	0.56	140	95

Table 2: Mole fractions for $NH_3/H_2/N_2$ fuel mixtures, fuel and air velocities, nominal and fitted strain rates

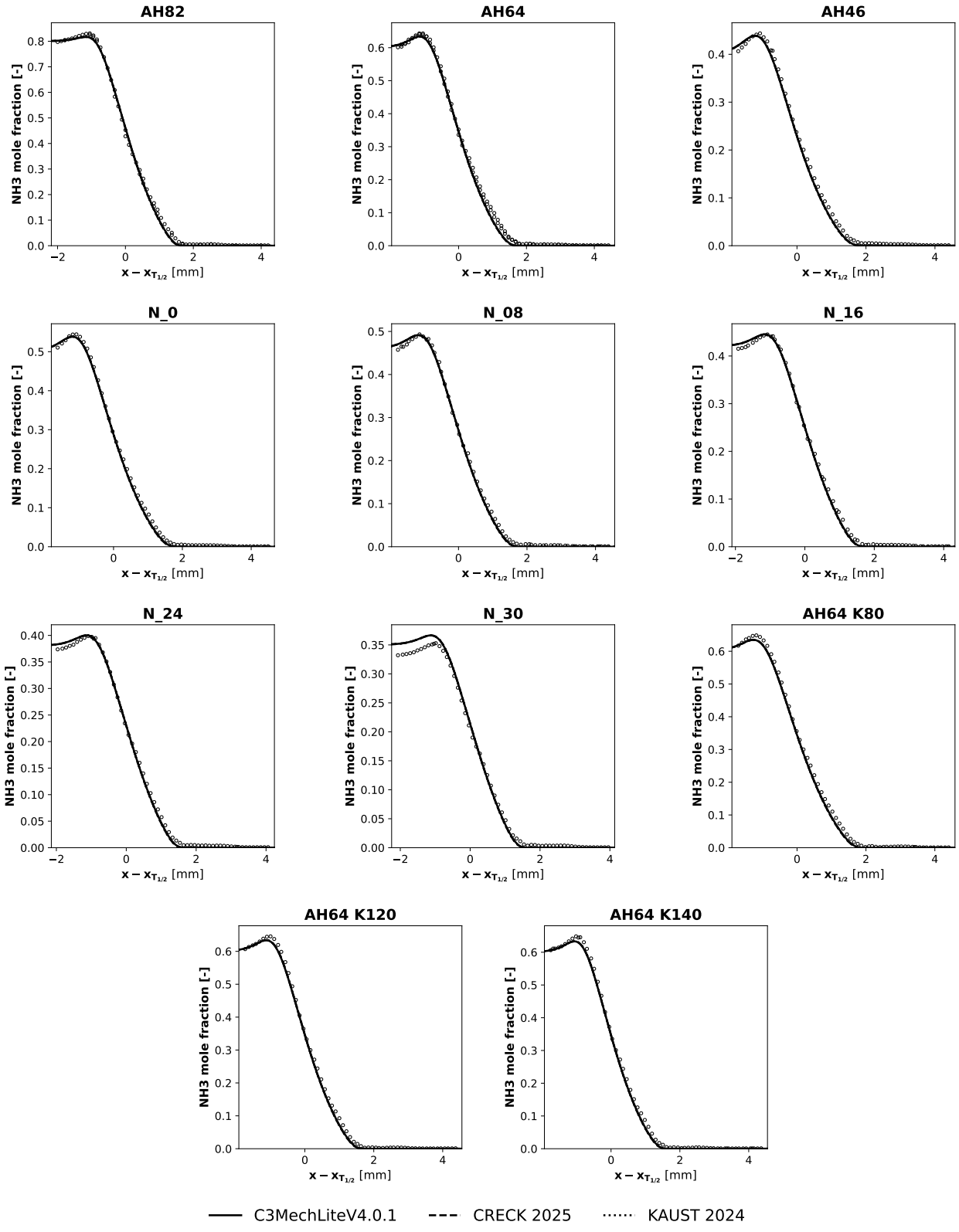

Figure 24: NH_3 profiles in a counterflow diffusion flame at atmospheric pressure, and variable compositions and strain rate (see Table 2).

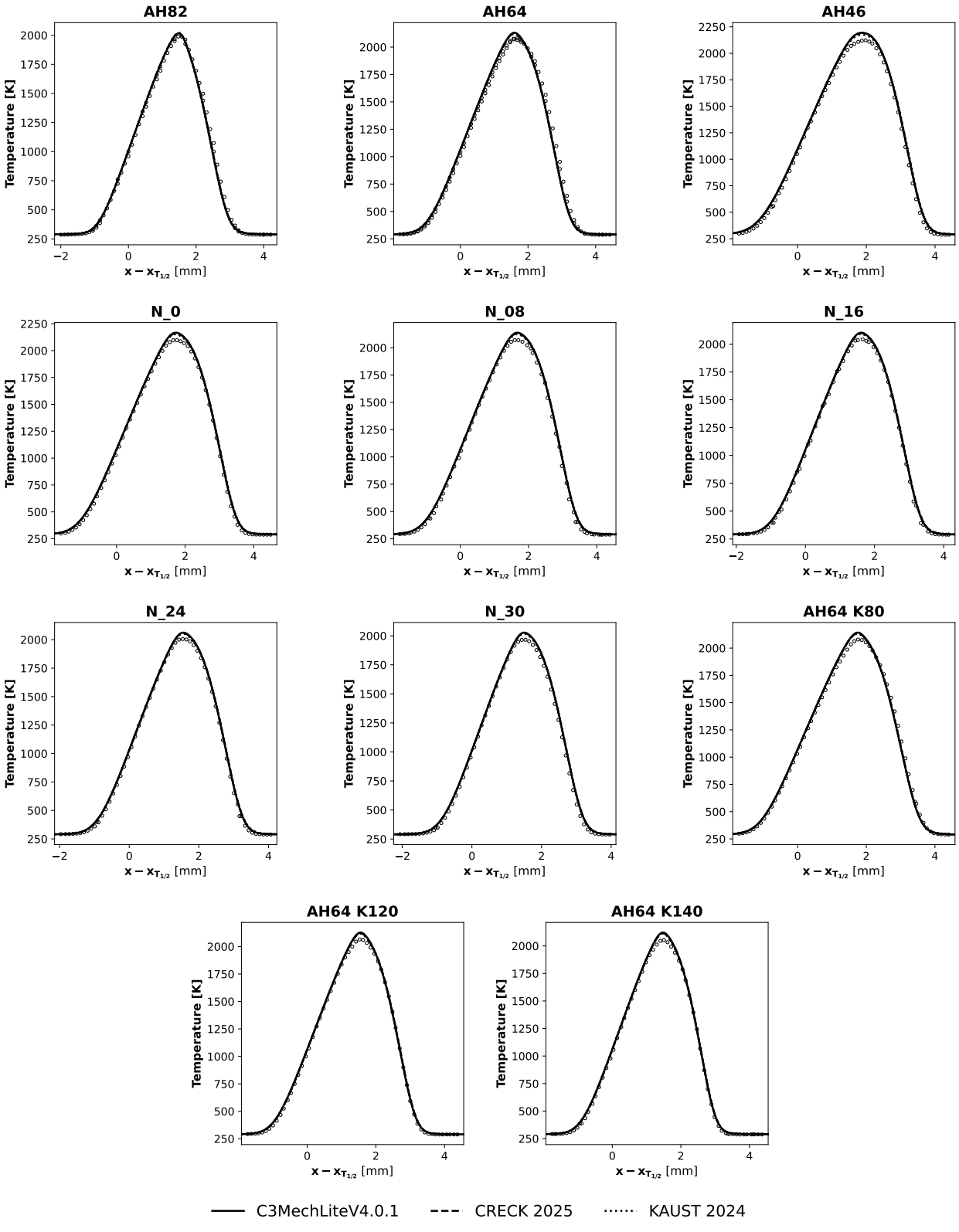

Figure 25: Temperature profiles in a counterflow diffusion flame at atmospheric pressure, and variable compositions and strain rate (see Table 2).

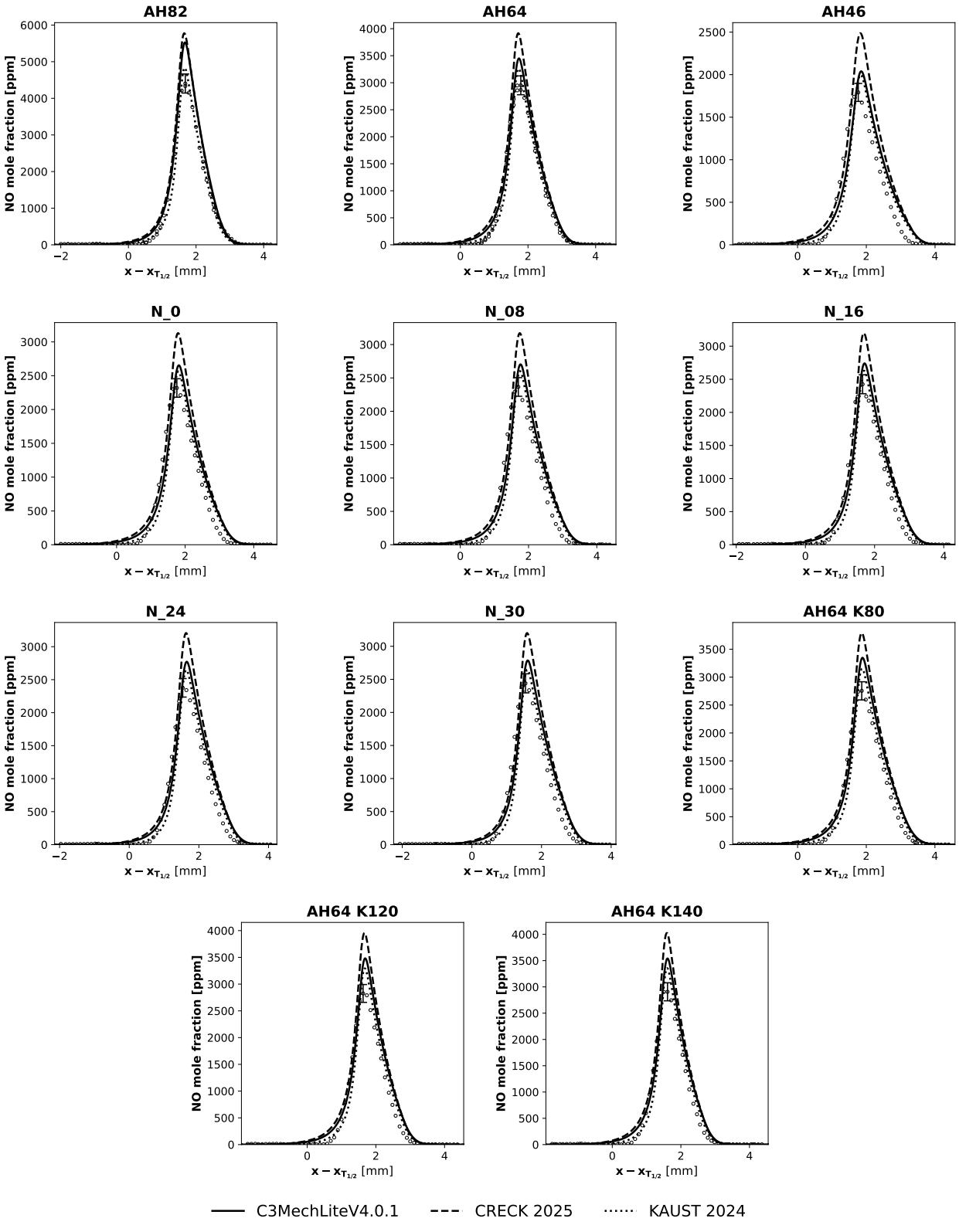

Figure 26: NO profiles in a counterflow diffusion flame at atmospheric pressure, and variable compositions and strain rate (see Table 2).

4.3.3 Hayakawa (2023) [16]

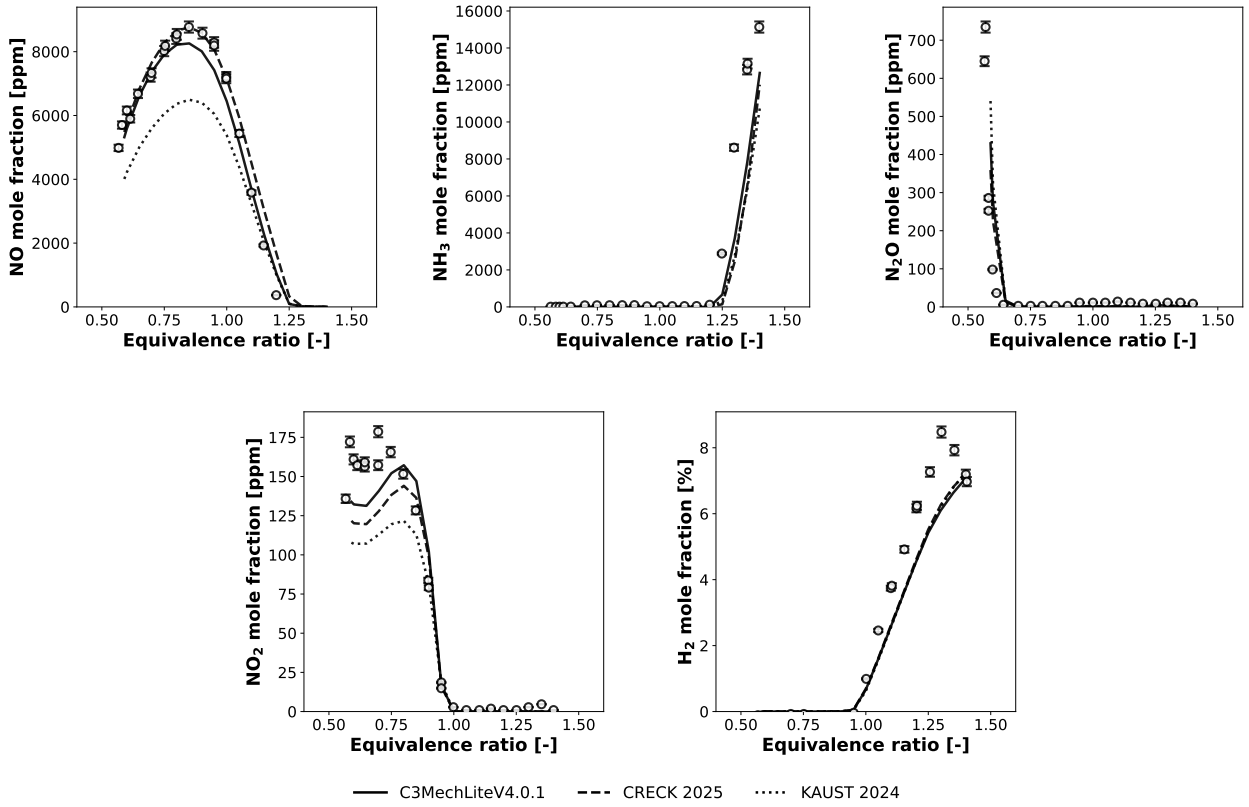

Figure 27: Emission features of a NH_3/H_2/air premixed laminar flame stabilized in a stagnation flow, as a function of the equivalence ratio. NH_3:H_2 = 70:30, P = 1 atm, T_{inlet} = 295 K.

4.3.4 Richter (2023) [17]

Following the procedure indicated in [17], NO mole fractions were evaluated 10 mm downstream of the maximum temperature gradient. The fuel velocity was equal to its laminar flame speed at ambient conditions.

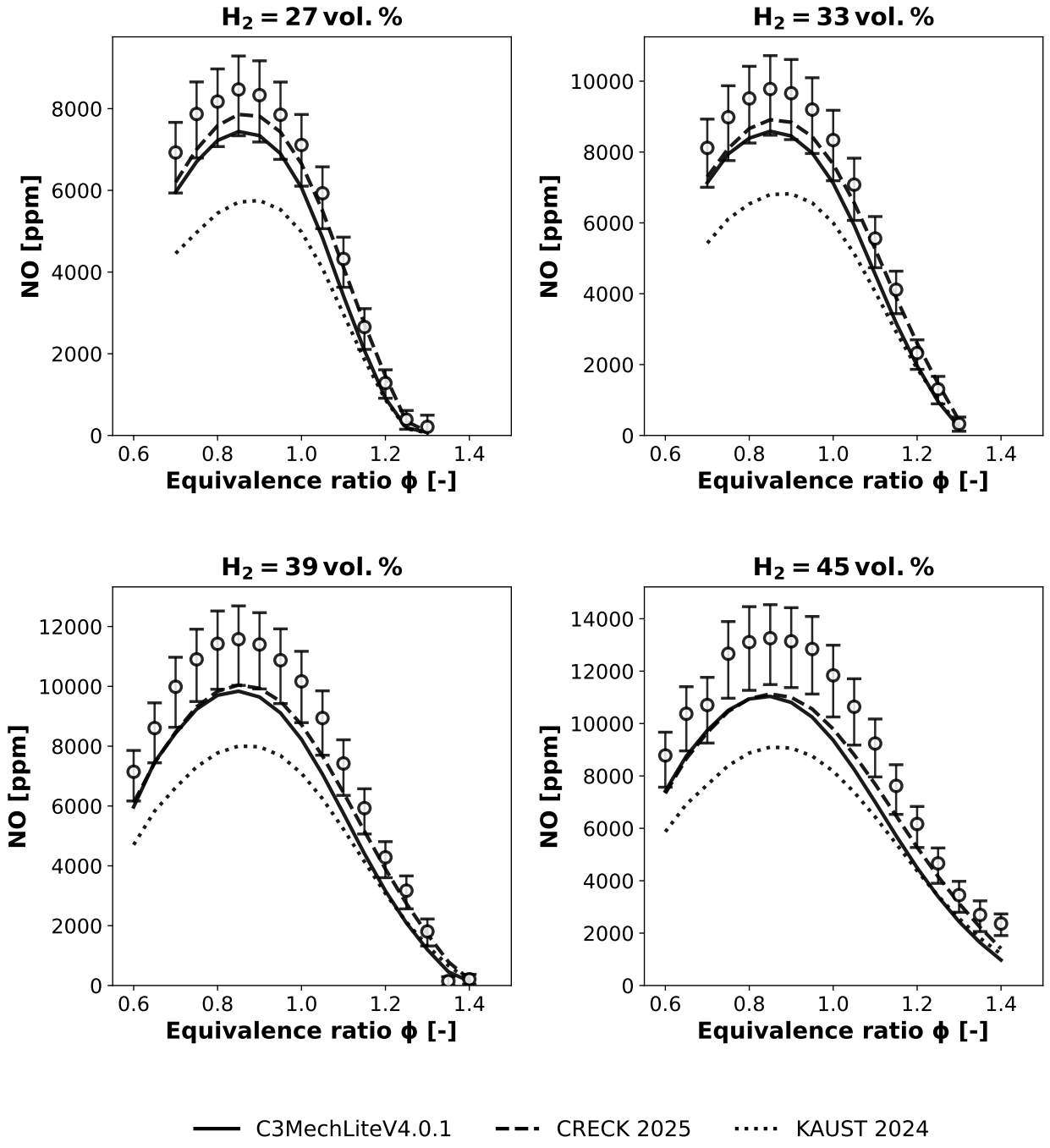

Figure 28: NO mole fraction profiles in the post-flame region of laminar premixed $NH_3/H_2/N_2$/air flames at atmospheric pressure, and variable X_{H_2}. P = 1 atm. T_u = 298 K.

4.3.5 Alturaifi (2022) [18]

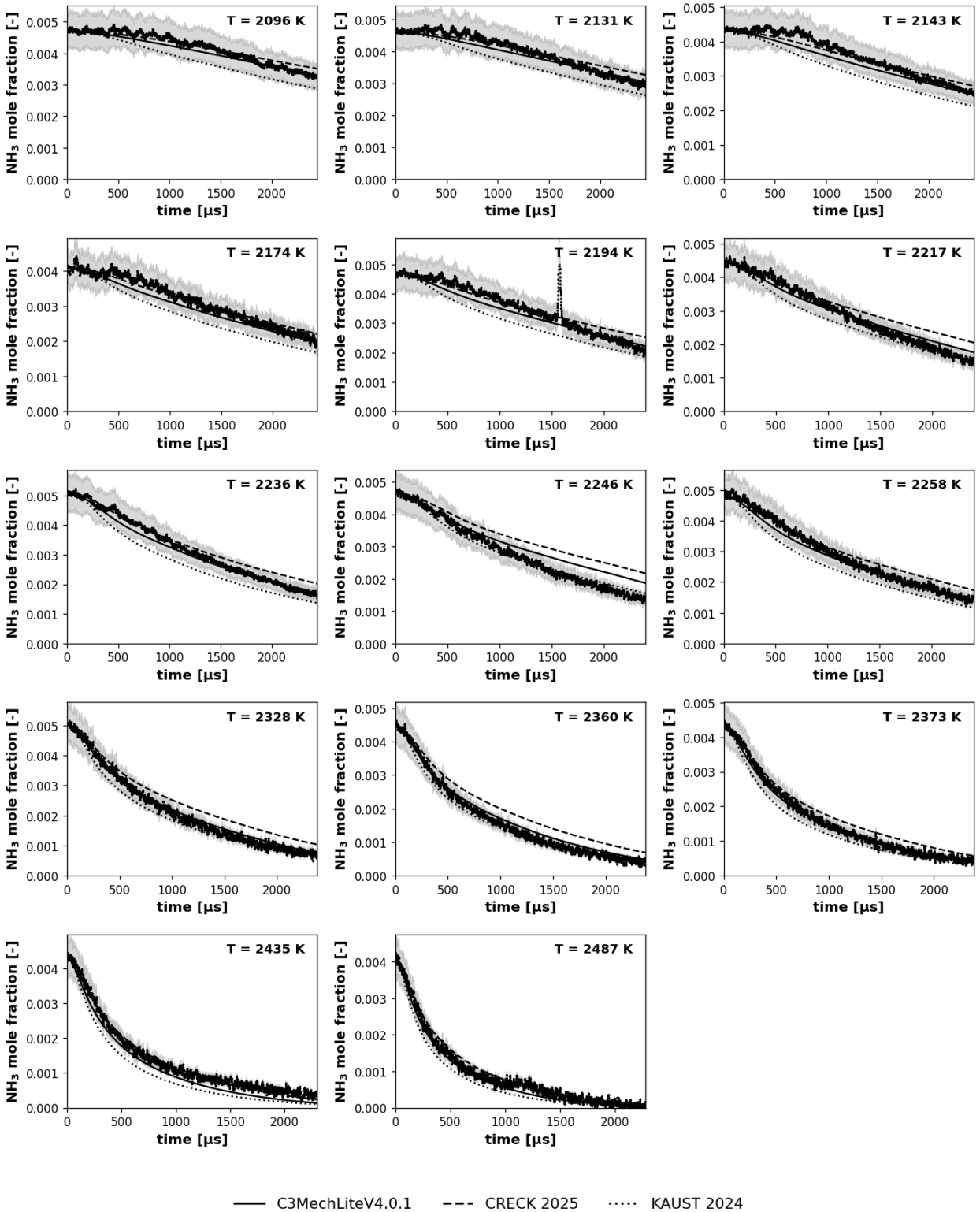

Figure 29: NH_3 species profile for a mixture of ~0.5% NH_3 in Ar, near atmospheric pressure.

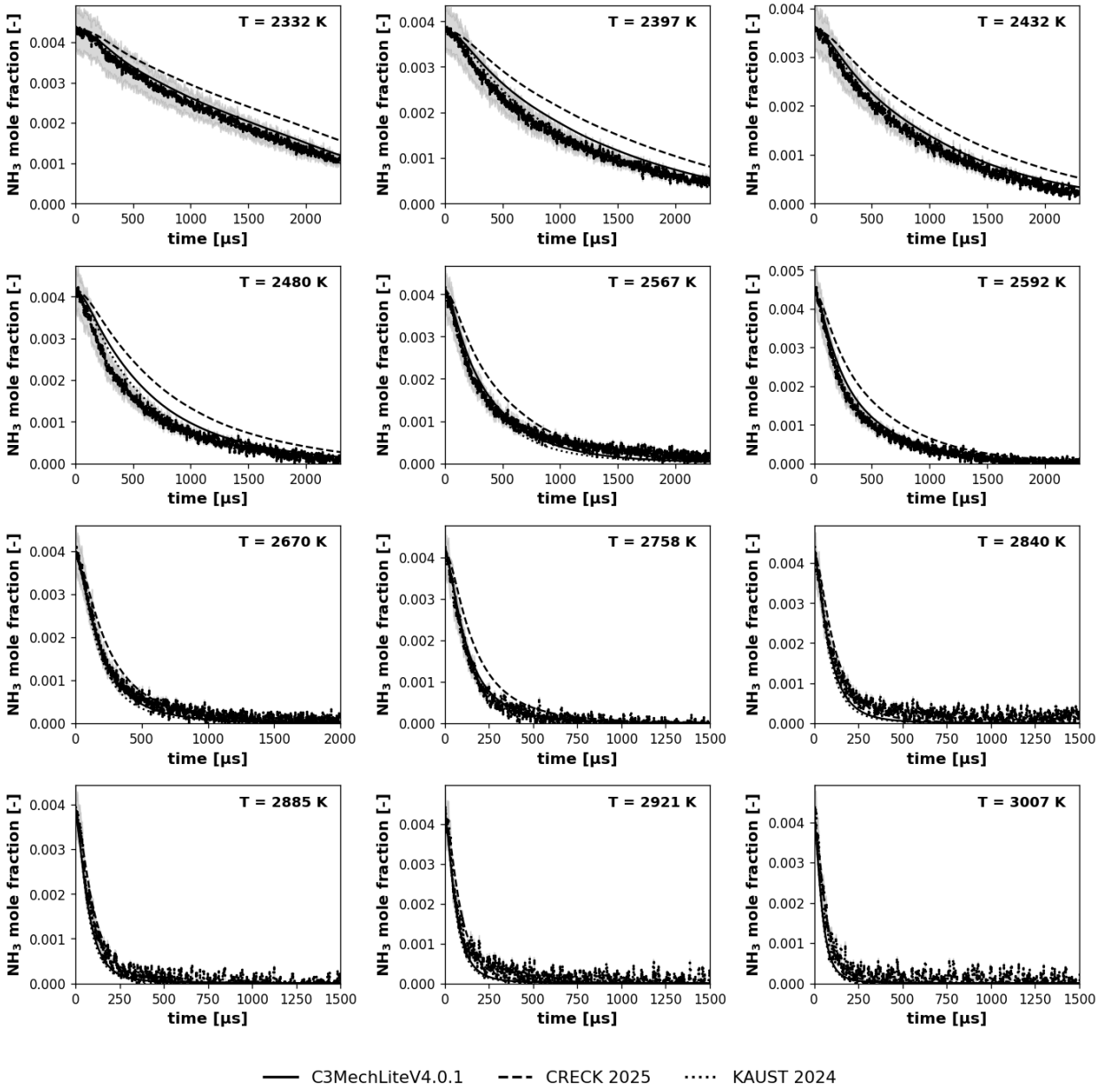

Figure 30: NH_3 species profile for a mixture of ∼0.42% NH_3/H_2 in Ar, near atmospheric pressure.

4.3.6 Alturaifi (2023) [19]

Mix ID	ϕ	NH_3:H_2	X_{NH_3}	X_{H_2}	X_{O_2}	X_{Ar}
1	0.58	100:0	0.00439	0	0.00569	0.98992
2	0.90	100:0	0.00536	0	0.00447	0.99017
3	1.06	100:0	0.00596	0	0.00423	0.98981
4	2.03	100:0	0.00732	0	0.00271	0.98997
5	1.07	80:20	0.00447	0.00117	0.00328	0.99108
6	1.02	50:50	0.00268	0.00254	0.00320	0.99158

Table 3: Mixture compositions investigated by Alturaifi et al. [19]. P $\approx$ 1.2 atm. 1474 K $\leq$ T $\leq$ 2307 K.

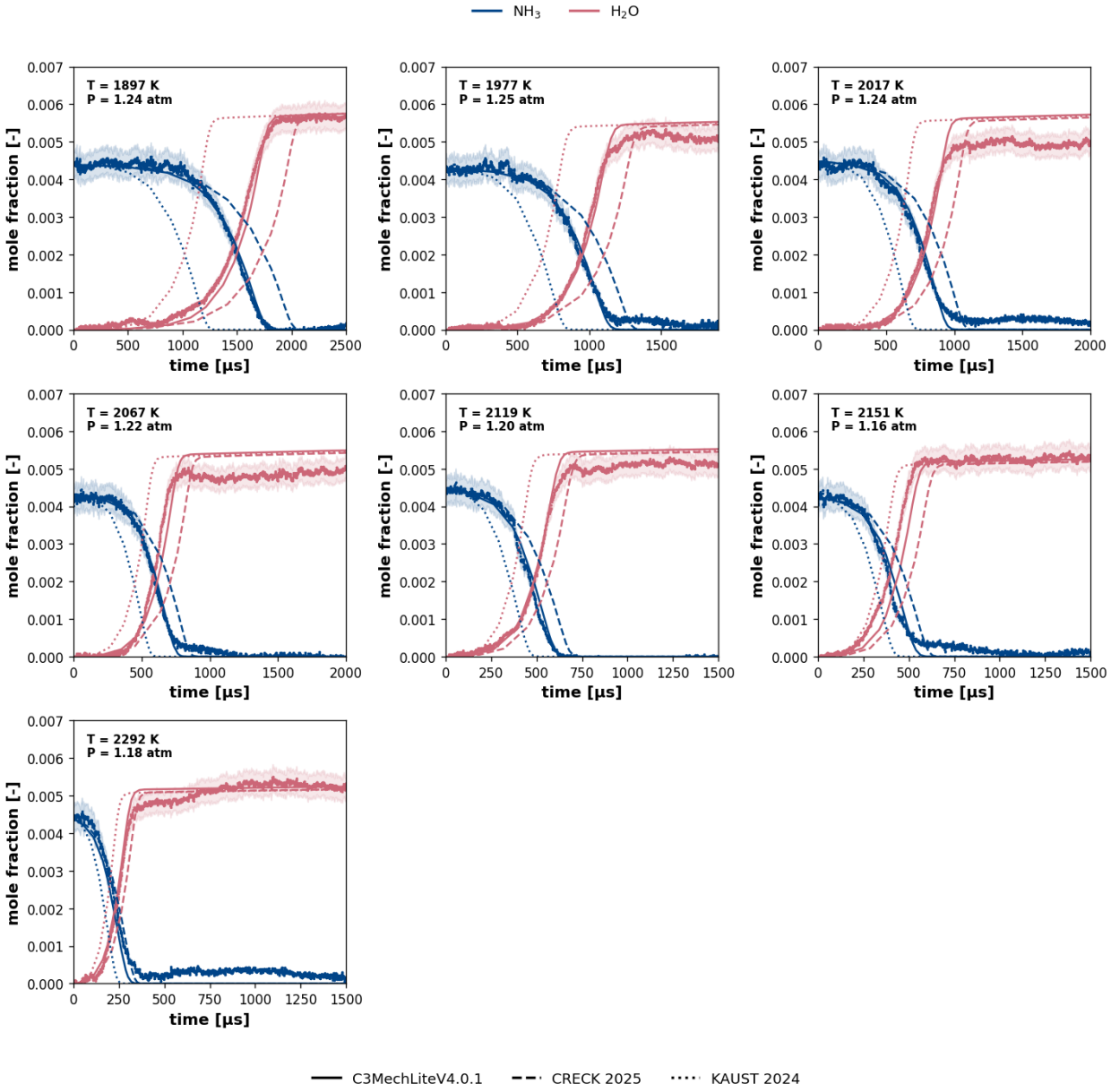

Figure 31: NH_3 and H_2O species profiles for mixture 1 (Table 3).

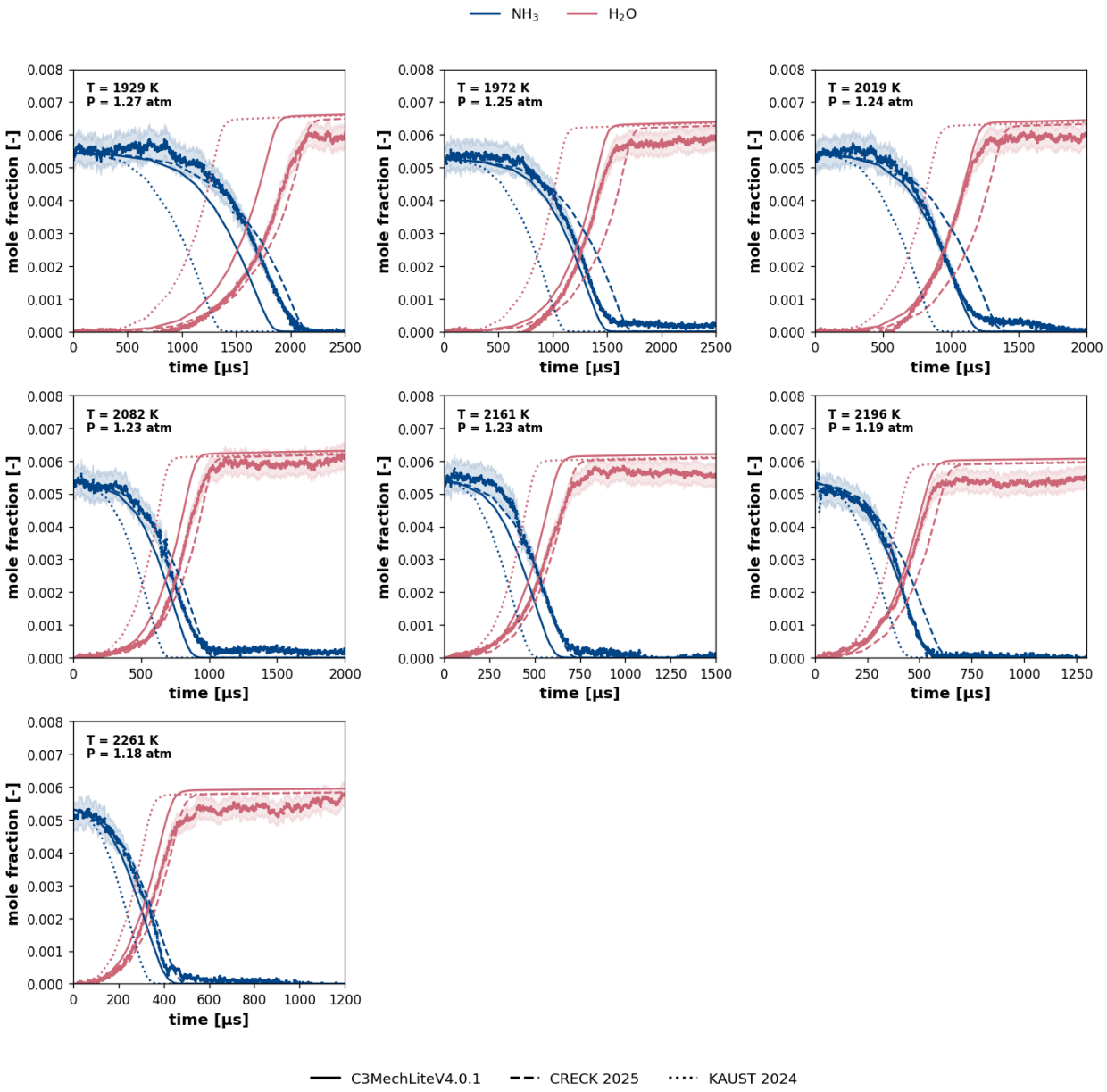

Figure 32: NH_3 and H_2O species profiles for mixture 2 (Table 3).

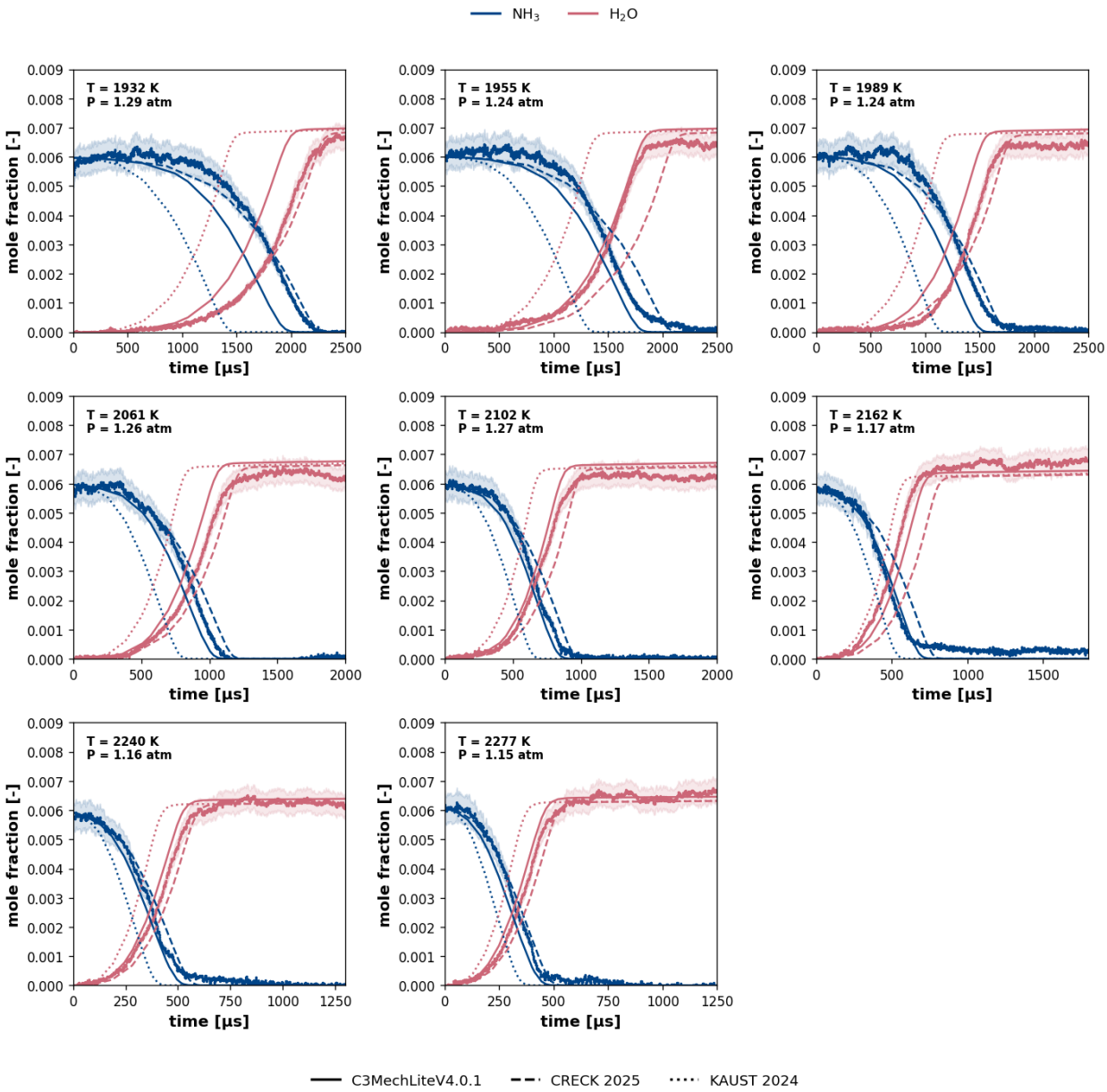

Figure 33: NH_3 and H_2O species profiles for mixture 3 (Table 3).

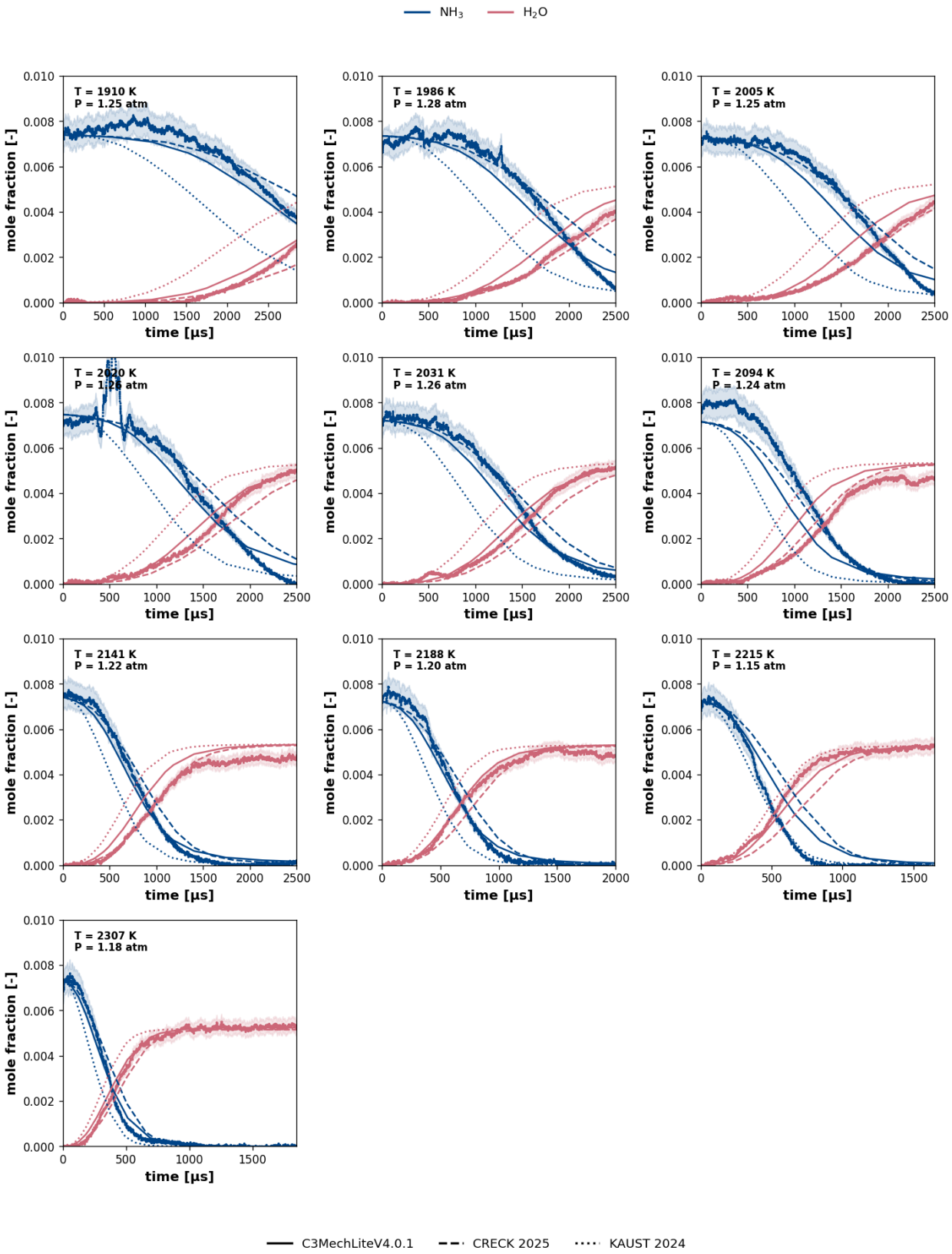

Figure 34: NH_3 and H_2O species profiles for mixture 4 (Table 3).

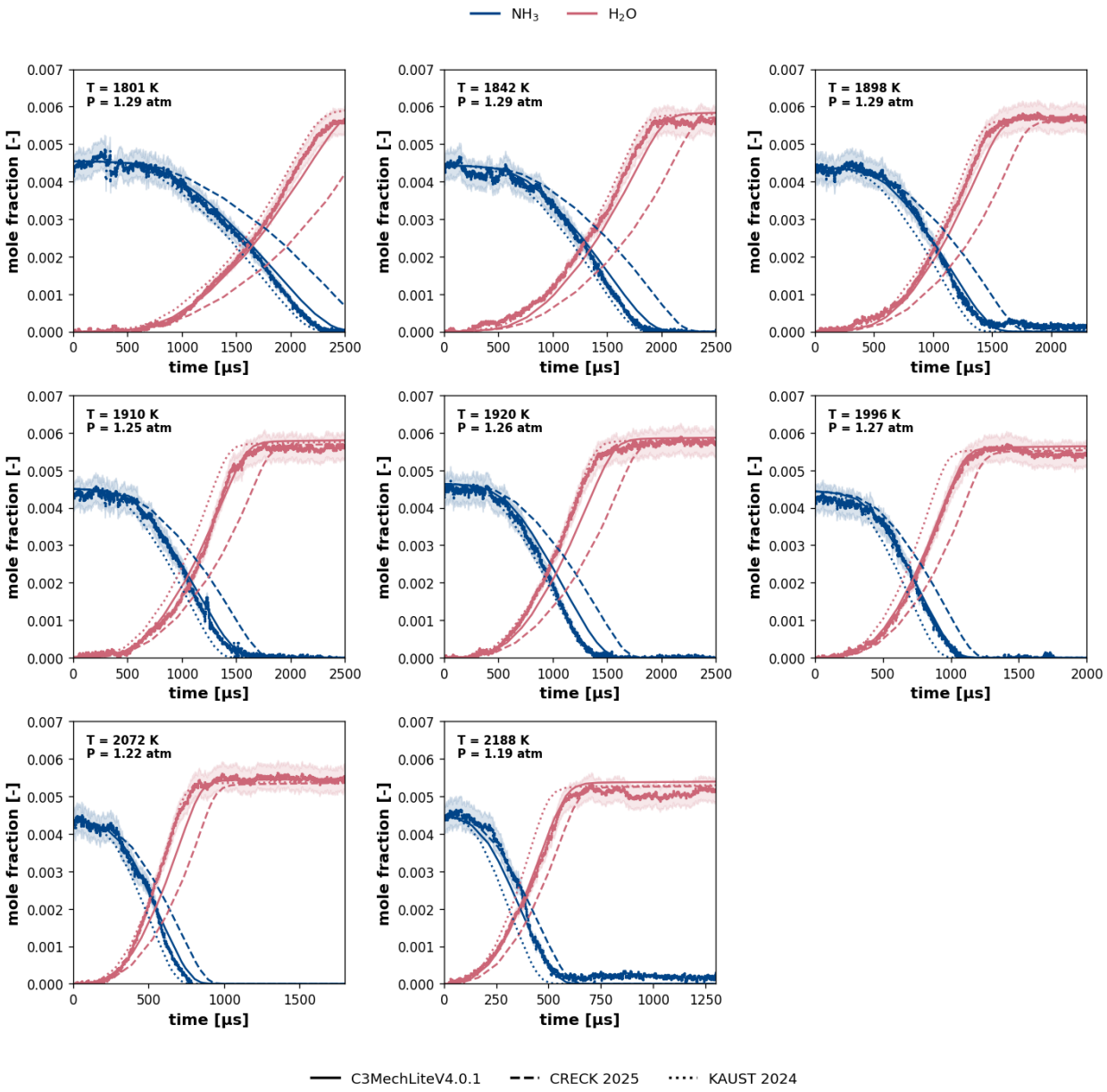

Figure 35: NH_3 and H_2O species profiles for mixture 5 (Table 3).

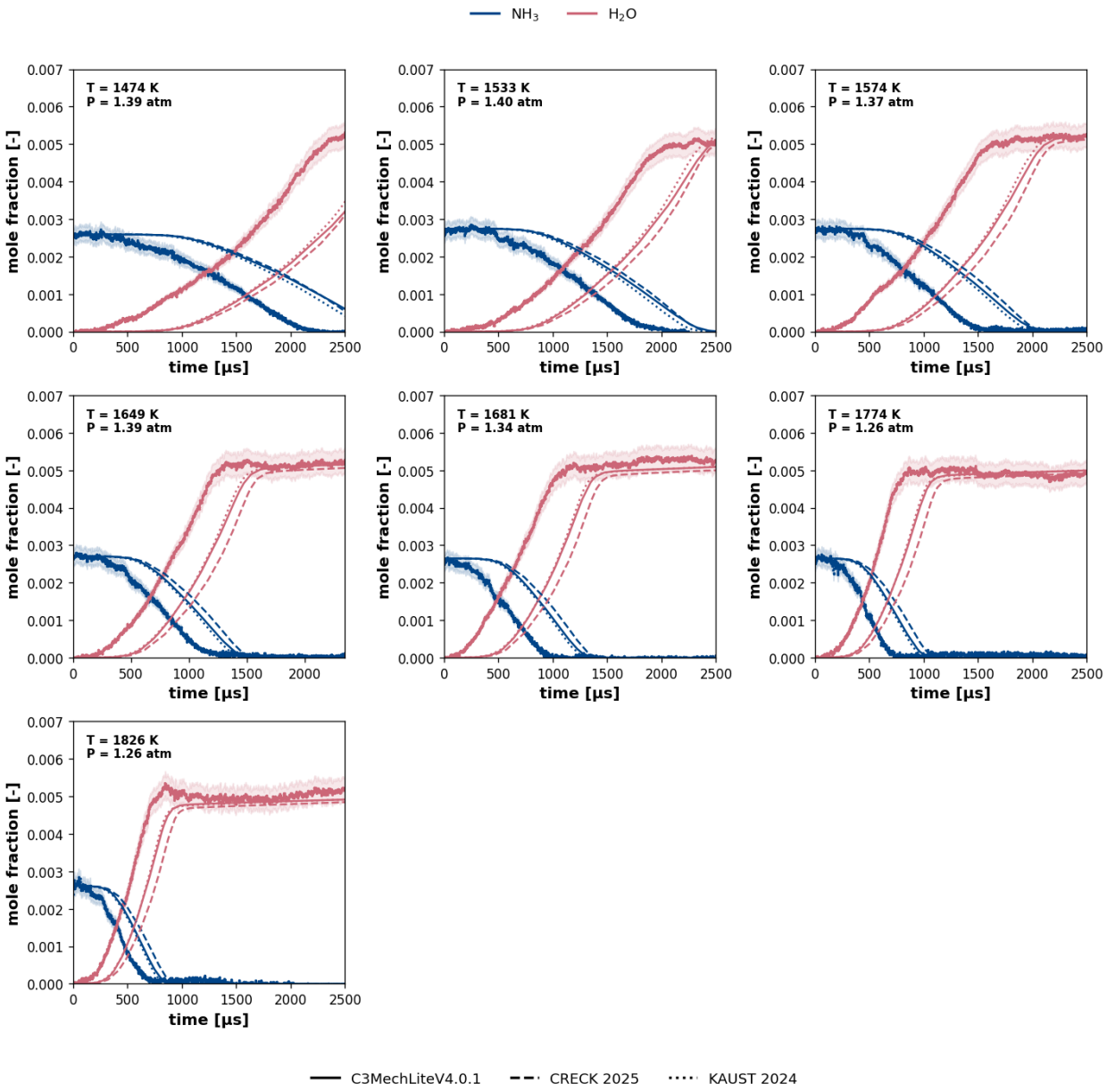

Figure 36: NH_3 and H_2O species profiles for mixture 6 (Table 3).

4.3.7 Alturaifi (2022) [20]

Mix ID	ϕ	$\mathbf{X}_{NH_3}$	$\mathbf{X}_{O_2}$	$\mathbf{X}_{Ar}$
1	0.54	0.01401	0.01948	0.96652
2	1.03	0.01948	0.01421	0.96631
3	1.84	0.02329	0.00957	0.96714

Table 4: Average mixture compositions investigated by Alturaifi et al. [20]. P $\approx$ 1.22 atm. 1829 K $\leq$ T $\leq$ 2198 K.

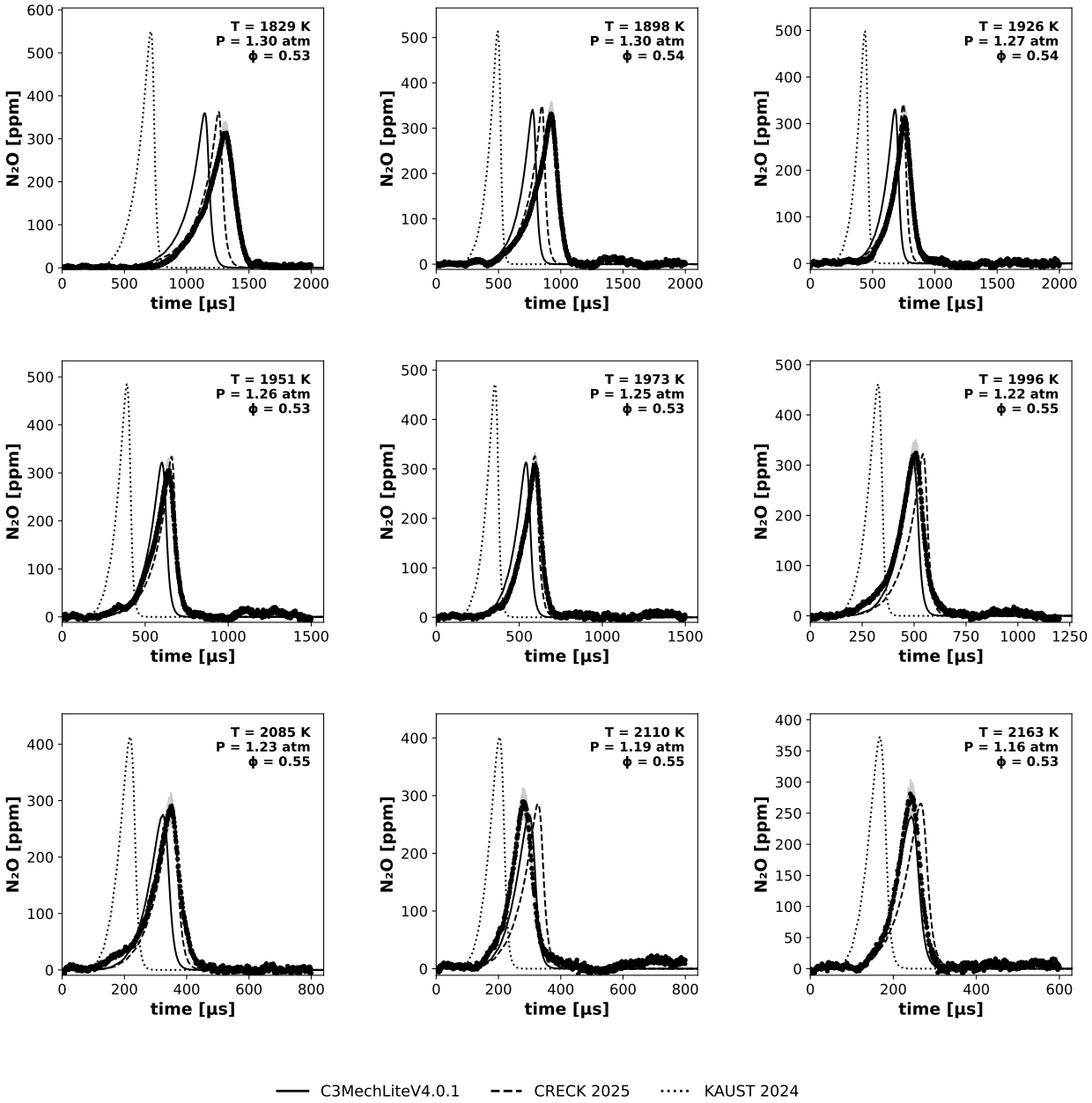

Figure 37: N_2O species profiles for mixture 1 (Table 4)

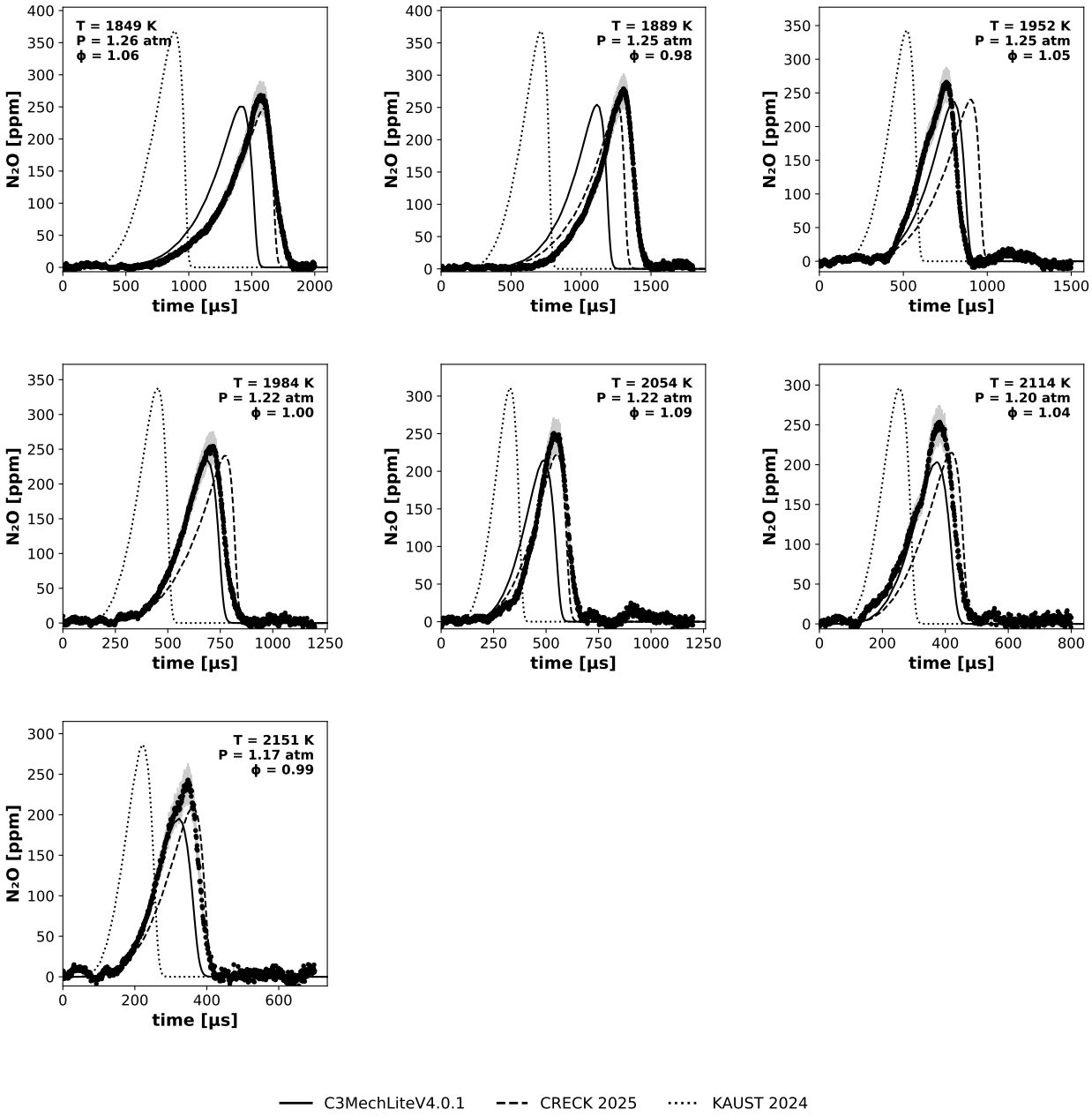

Figure 38: N_2O species profiles for mixture 2 (Table 4)

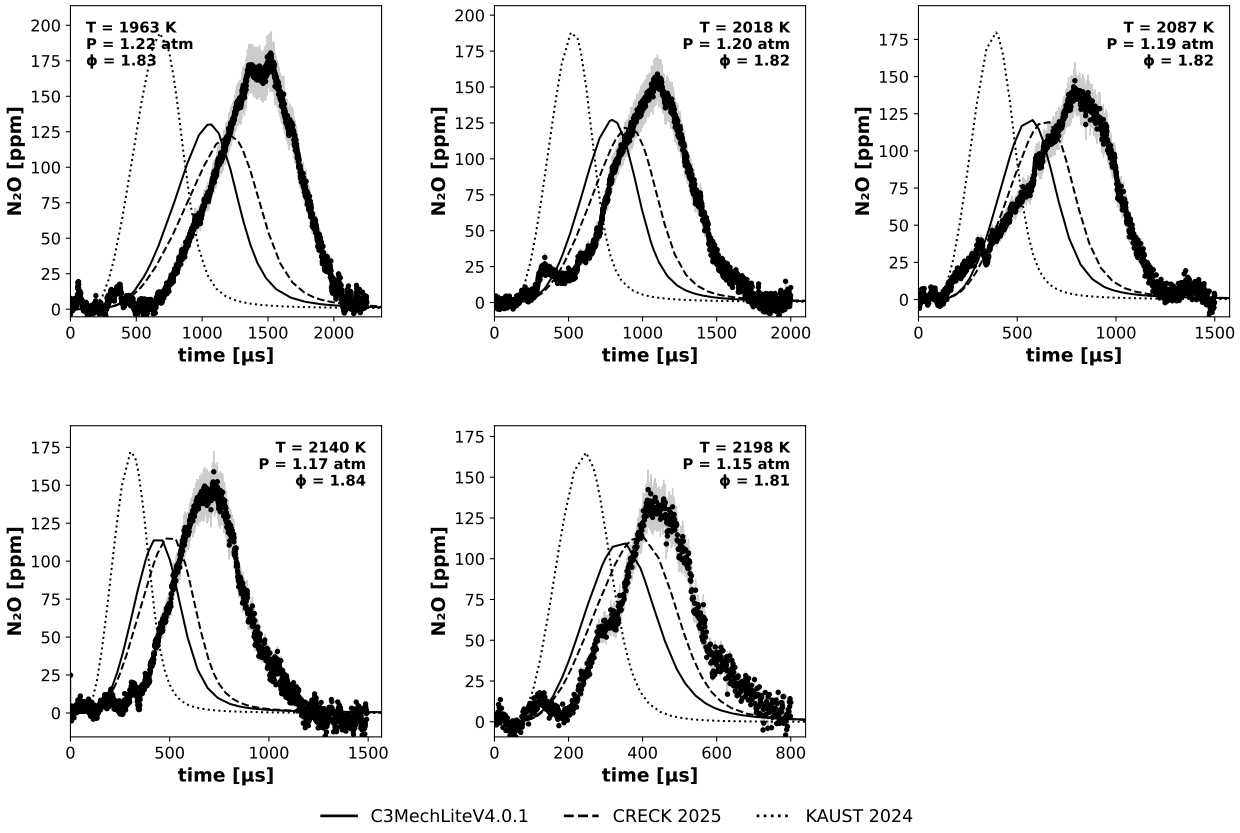

Figure 39: N_2O species profiles for mixture 3 (Table 4)

4.3.8 Mathieu (2024) [21]

Mix ID	ϕ	$\mathbf{X}_{\mathrm{NH_3}}$	$\mathbf{X}_{\mathrm{N_2O}}$	$\mathbf{X}_{\mathrm{Ar}}$
1	0.25	0.00070	0.00430	0.99500
2	0.85	0.00178	0.00322	0.99500
3	1.00	0.00199	0.00301	0.99500
4	2.00	0.00286	0.00214	0.99500

Table 5: Average mixture compositions investigated by Mathieu et al. [21]. $1.25\,\mathrm{atm} \leq \mathrm{P} \leq 1.47\,\mathrm{atm}$. $1458\,\mathrm{K} \leq \mathrm{T} \leq 2200\,\mathrm{K}$.

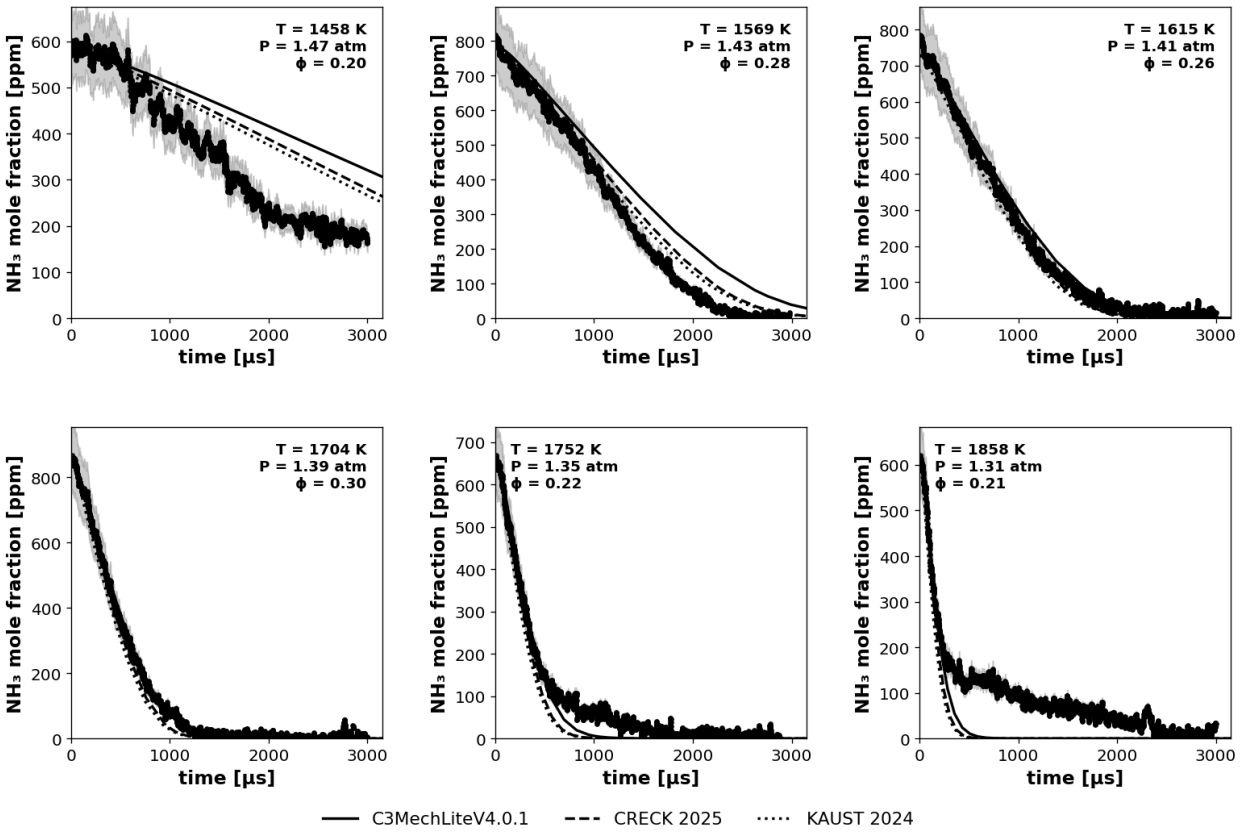

Figure 40: NH_3 species profiles for mixture 1 (Table 5)

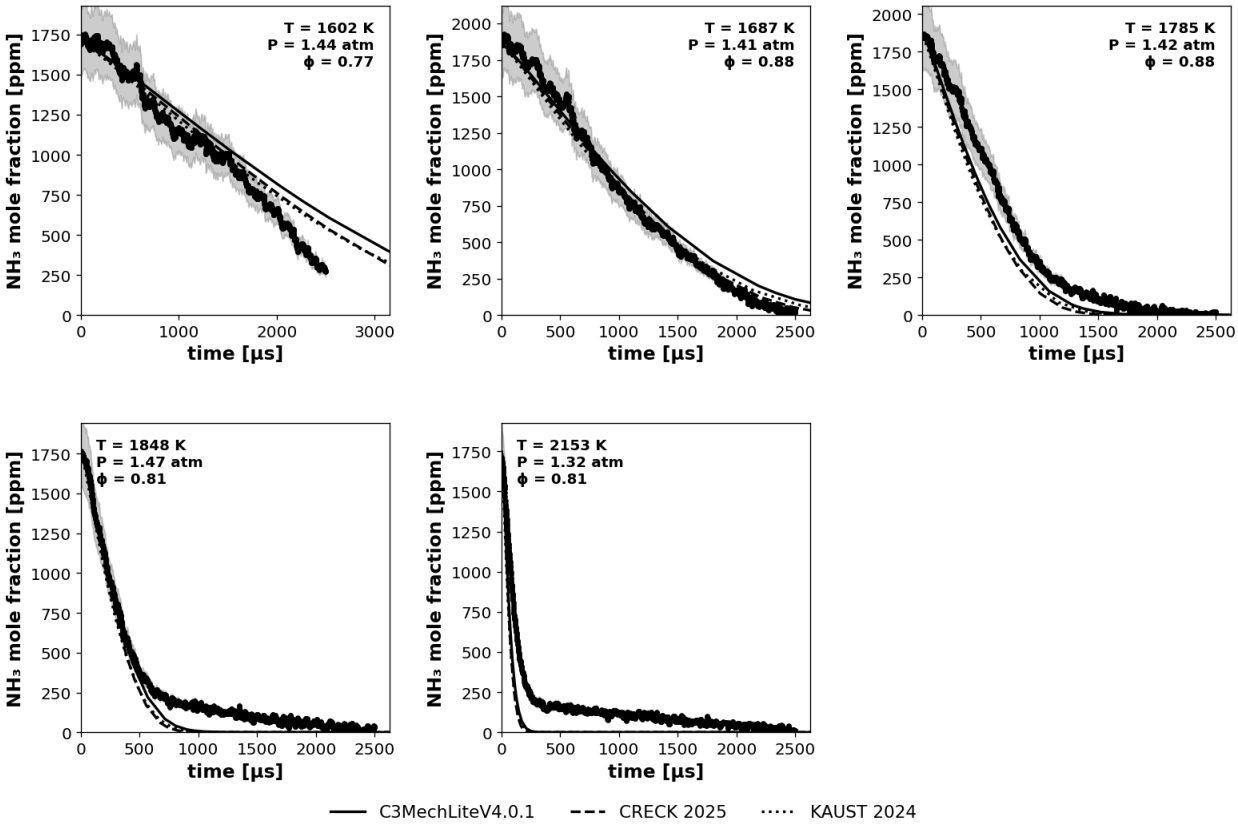

Figure 41: NH_3 species profiles for mixture 2 (Table 5)

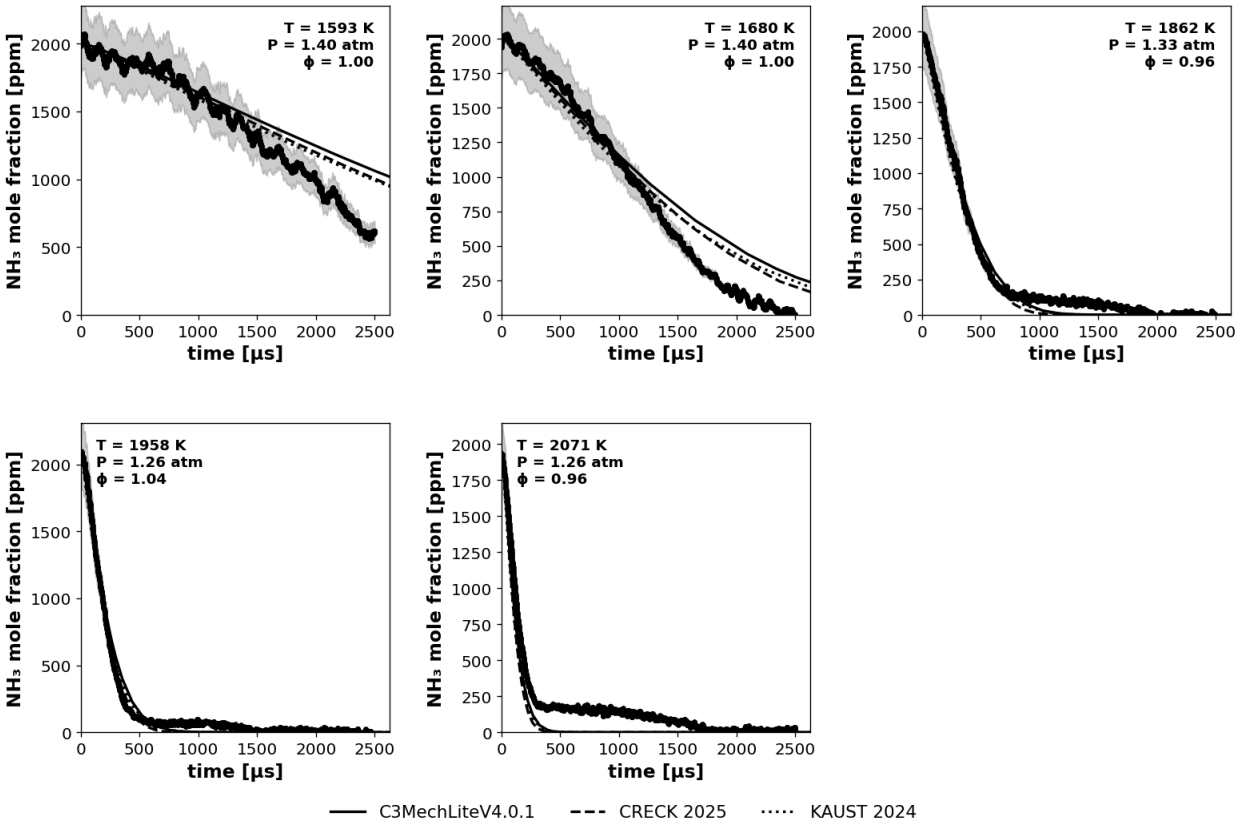

Figure 42: NH_3 species profiles for mixture 3 (Table 5)

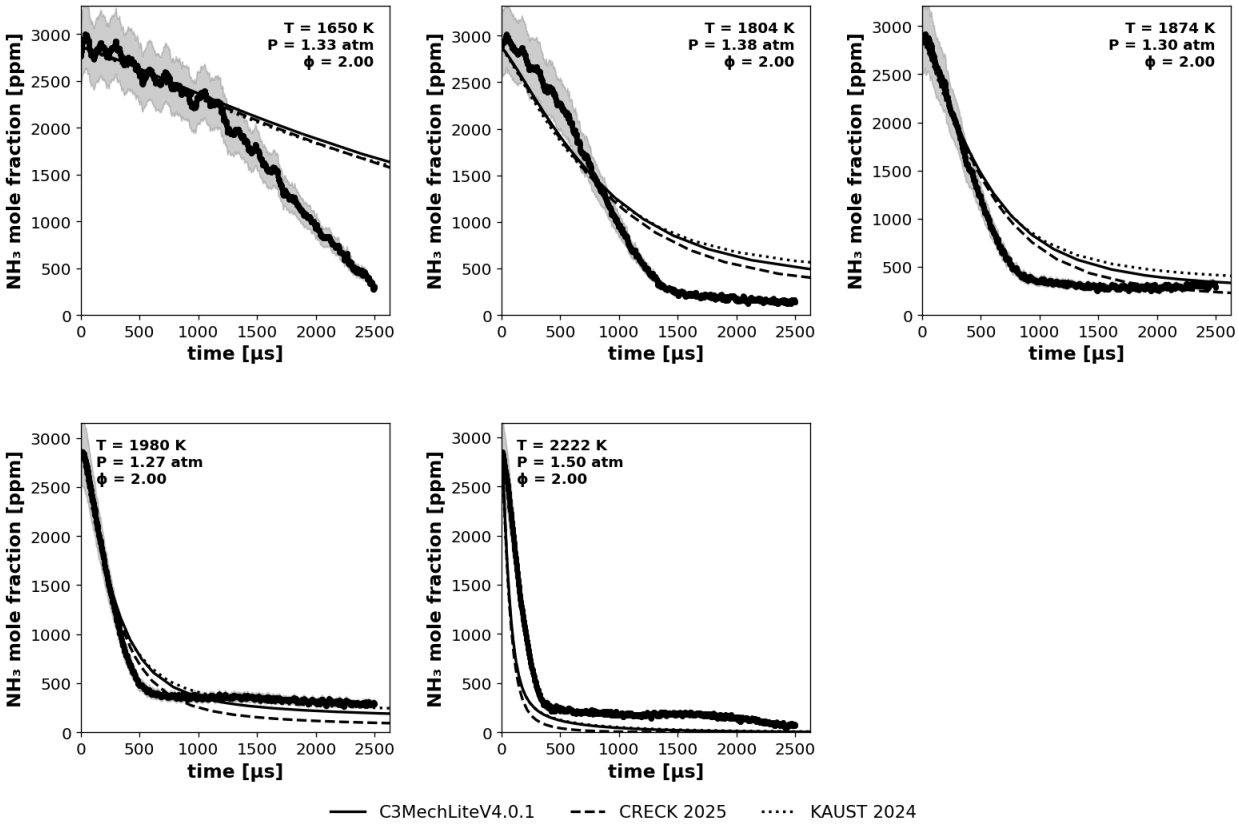

Figure 43: NH_3 species profiles for mixture 4 (Table 5)

References

[1] M. Figueroa-Labastida, L. Zheng, A. M. Ferris, N. Obrecht, C. Callu, R. K. Hanson, Shock-tube laminar flame speed measurements of ammonia/airgon mixtures at temperatures up to 771 K, Combustion and Flame 260 (2024) 113256.

[2] M. Figueroa-Labastida, L. Zheng, J. W. Streicher, R. K. Hanson, Ammonia/hydrogen laminar flame speed measurements at elevated temperatures, International Journal of Hydrogen Energy 63 (2024) 1137–1146.

[3] C. Lhuillier, P. Brequigny, N. Lamoureux, F. Contino, C. Mounaïm-Rousselle, Experimental investigation on laminar burning velocities of ammonia/hydrogen/air mixtures at elevated temperatures, Fuel 263 (2020) 116653.

[4] K. P. Shrestha, C. Lhuillier, A. A. Barbosa, P. Brequigny, F. Contino, C. Mounaïm-Rousselle, L. Seidel, F. Mauss, An experimental and modeling study of ammonia with enriched oxygen content and ammonia/hydrogen laminar flame speed at elevated pressure and temperature, Proceedings of the Combustion Institute 38 (2021) 2163–2174.

[5] R. Kanoshima, A. Hayakawa, T. Kudo, E. C. Okafor, S. Colson, A. Ichikawa, T. Kudo, H. Kobayashi, Effects of initial mixture temperature and pressure on laminar burning velocity and markstein length of ammonia/air premixed laminar flames, Fuel 310 (2022) 122149.

[6] B. Mei, J. Zhang, X. Shi, Z. Xi, Y. Li, Enhancement of ammonia combustion with partial fuel cracking strategy: Laminar flame propagation and kinetic modeling investigation of nh3/h2/n2/air mixtures up to 10 atm, Combustion and flame 231 (2021) 111472.

[7] Q. Liu, X. Chen, J. Huang, Y. Shen, Y. Zhang, Z. Liu, The characteristics of flame propagation in ammonia/oxygen mixtures, Journal of hazardous materials 363 (2019) 187–196.

[8] B. Mei, X. Zhang, S. Ma, M. Cui, H. Guo, Z. Cao, Y. Li, Experimental and kinetic modeling investigation on the laminar flame propagation of ammonia under oxygen enrichment and elevated pressure conditions, Combustion and Flame 210 (2019) 236–246.

[9] G. J. Gotama, A. Hayakawa, E. C. Okafor, R. Kanoshima, M. Hayashi, T. Kudo, H. Kobayashi, Measurement of the laminar burning velocity and kinetics study of the importance of the hydrogen recovery mechanism of ammonia/hydrogen/air premixed flames, Combustion and Flame 236 (2022) 111753.

[10] A. Hamadi, N. Obrecht, C. Callu, A. Stagni, T. Faravelli, A. Comandini, N. Chaumeix, Experimental and modeling investigation of the laminar flame speeds for ammonia with various oxygen and diluent mixtures, Proceedings of the Combustion Institute 40 (2024) 105387.

[11] B. Liu, Z. Zhang, M. Zhou, G. Li, Laminar flames and chemical kinetics analysis of NH_3/NO and NH_3/N_2O mixtures in the absence of oxygen, Combustion and Flame 279 (2025) 114341.

[12] N. Wang, T. Li, X. Guo, Z. Wu, S. Huang, X. Zhou, S. Li, R. Chen, Laminar burning characteristics of ammonia and hydrogen blends at elevated initial pressures up to 2.5 mpa, Chemical Engineering Journal 500 (2024) 157283.

[13] S. Wang, Z. Wang, A. M. Elbaz, X. Han, Y. He, M. Costa, A. A. Konnov, W. L. Roberts, Experimental study and kinetic analysis of the laminar burning velocity of NH_3/syngas/air, NH_3/CO/air and NH_3/H_2/air premixed flames at elevated pressures, Combustion and Flame 221 (2020) 270–287.

[14] D. E. Thomas, K. P. Shrestha, F. Mauss, W. F. Northrop, Extinction and no formation of ammonia-hydrogen and air non-premixed counterflow flames, Proceedings of the Combustion Institute 39 (2023) 1803–1812.

[15] H. Tang, Z. Al Hadi, T. F. Guiberti, W. Sun, G. Magnotti, Experimental study of nitric oxide distributions in non-premixed and premixed ammonia/hydrogen-air counterflow flames, Combustion and Flame 267 (2024) 113556.

[16] A. Hayakawa, M. Hayashi, M. Kovaleva, G. J. Gotama, E. C. Okafor, S. Colson, S. Mashruk, A. Valera-Medina, T. Kudo, H. Kobayashi, Experimental and numerical study of product gas and N_2O emission characteristics of ammonia/hydrogen/air premixed laminar flames stabilized in a stagnation flow, Proceedings of the Combustion Institute 39 (2023) 1625–1633.

[17] M. Richter, J. Lill, R. Barlow, A. Gruber, A. Dreizler, J. Dawson, D. Geyer, Quantification of no in the post-flame region of laminar premixed ammonia/hydrogen/nitrogen-air flames using laser induced fluorescence, Combustion and Flame 277 (2025) 114139.

[18] S. A. Alturaifi, O. Mathieu, E. L. Petersen, An experimental and modeling study of ammonia pyrolysis, Combustion and Flame 235 (2022) 111694.

[19] S. A. Alturaifi, O. Mathieu, E. L. Petersen, A shock-tube study of NH_3 and NH_3/H_2 oxidation using laser absorption of NH_3 and H_2O, Proceedings of the Combustion Institute 39 (2023) 233–241.

[20] S. A. Alturaifi, O. Mathieu, E. L. Petersen, Shock-tube laser absorption measurements of N_2O time histories during ammonia oxidation, Fuel Communications 10 (2022) 100050.

[21] O. Mathieu, C. M. Grégoire, E. L. Petersen, Shock-tube study of the oxidation of ammonia by N_2O, Proceedings of the Combustion Institute 40 (2024) 105250.

[22] D. G. Goodwin, H. K. Moffat, I. Schoegl, R. L. Speth, B. W. Weber, Cantera: An object-oriented software toolkit for chemical kinetics, thermodynamics, and transport processes, `https://www.cantera.org`, 2025. doi:`10.5281/zenodo.14455267`, version 3.2.0.

[23] A. Cuoci, A. Frassoldati, T. Faravelli, E. Ranzi, OpenSMOKE++: An object-oriented framework for the numerical modeling of reactive systems with detailed kinetic mechanisms, Computer Physics Communications 192 (2015) 237–264.

[24] R. Langer, A. Cuoci, L. Cai, U. Burke, C. Olm, H. Curran, T. Turányi, H. Pitsch, et al., A comparison of numerical frameworks for modelling homogenous reactors and laminar flames, in: Joint Meeting: The German and Italian Sections of the Combustion Institute, ITA, 2018, pp. 9–14.

[25] H. Nakamura, M. Shindo, Effects of radiation heat loss on laminar premixed ammonia/air flames, Proceedings of the Combustion Institute 37 (2019) 1741–1748.

[26] A. Stagni, F. R. Artioli, A. Frassoldati, The role of radiative heat loss and collisional energy transfer in the flammability limits of NH_3 and NH_3–H_2 mixtures, Industrial & Engineering Chemistry Research 63 (2024) 21805–21815.

[27] Y. Murakami, Q.-D. Wang, S. Liu, Y. Zhu, P. Wang, L. P. Maffei, R. Langer, T. Faravelli, H. Pitsch, S. J. Klippenstein, et al., C3mechlite: An integrated component library of compact kinetic mechanisms for low-carbon, carbon neutral and zero-carbon fuels, Combustion and Flame 282 (2025) 114410.

[28] Y. Zhu, H. J. Curran, S. Girhe, Y. Murakami, H. Pitsch, K. Senecal, L. Yang, C.-W. Zhou, The combustion chemistry of ammonia and ammonia/hydrogen mixtures: A comprehensive chemical kinetic modeling study, Combustion and Flame 260 (2024) 113239.

[29] L. P. Maffei, R. Langer, Y. Murakami, S. W. Wagnon, P. Wang, J. Liu, M. Raza, Y. Zhu, S. Girhe, C. Schwenzer, et al., Modeling combustion chemistry using c3mechv4. 0: an extension to mixtures of hydrogen, ammonia, alkanes, and cycloalkanes, Applications in Energy and Combustion Science (2025) 100385.

[30] A. Stagni, T. Dinelli, Impact of third-body colliders on ammonia pyrolysis and oxidation: Detailed kinetic modeling and mechanistic insights, Chemical Engineering Journal (2025) 170737.

[31] A. Stagni, C. Cavallotti, S. Arunthanayothin, Y. Song, O. Herbinet, F. Battin-Leclerc, T. Faravelli, An experimental, theoretical and kinetic-modeling study of the gas-phase oxidation of ammonia, Reaction Chemistry & Engineering 5 (2020) 696–711.

[32] A. Stagni, S. Arunthanayothin, M. Dehue, O. Herbinet, F. Battin-Leclerc, P. Bréquigny, C. Mounaïm-Rousselle, T. Faravelli, Low-and intermediate-temperature ammonia/hydrogen oxidation in a flow reactor: Experiments and a wide-range kinetic modeling, Chemical Engineering Journal 471 (2023) 144577.

[33] M. Monge-Palacios, X. Zhang, N. Morlanes, H. Nakamura, G. Pezzella, S. M. Sarathy, Ammonia pyrolysis and oxidation chemistry, Progress in Energy and Combustion Science 105 (2024) 101177.

[34] X. Zhang, K. K. Yalamanchi, S. M. Sarathy, Combustion chemistry of ammonia/c1 fuels: A comprehensive kinetic modeling study, Fuel 341 (2023) 127676.

[35] X. Han, Z. Wang, M. Costa, Z. Sun, Y. He, K. Cen, Experimental and kinetic modeling study of laminar burning velocities of NH_3/air, NH_3/H_2/air, NH_3/CO/air and NH_3/CH_4/air premixed flames, Combustion and Flame 206 (2019) 214–226.

[36] K. Seshadri, F. Williams, Laminar flow between parallel plates with injection of a reactant at high reynolds number, International Journal of Heat and Mass Transfer 21 (1978) 251–253.